HHS Public Access

Author manuscript

*Science*. Author manuscript; available in PMC 2022 June 18.

Published in final edited form as:

*Science*. 2021 June 18; 372(6548): . doi:10.1126/science.abe7729.

# Neutrophils self-limit swarming to contain bacterial growth in vivo

**Korbinian Kienle**[1,2,3], **Katharina M. Glaser**[1,2,3], **Sarah Eickhoff**[4], **Michael Mihlan**[1], **Konrad Knöpper**[4], **Eduardo Reátegui**[5,6], **Maximilian W. Epple**[1,2,3], **Matthias Gunzer**[7,8], **Ralf Baumeister**[9], **Teresa K. Tarrant**[10], **Ronald N. Germain**[11], **Daniel Irimia**[5], **Wolfgang Kastenmüller**[4], **Tim Lämmermann**[1,*]

[1]Max Planck Institute of Immunobiology and Epigenetics, Freiburg, Germany.

[2]International Max Planck Research School for Immunobiology, Epigenetics and Metabolism (IMPRS-IEM), Freiburg, Germany.

[3]Faculty of Biology, University of Freiburg, Freiburg, Germany.

[4]Institute of Systems Immunology, University of Würzburg, Max Planck Research Group, Würzburg, Germany.

[5]Center for Engineering in Medicine, Massachusetts General Hospital, Harvard Medical School, Shriners Hospital for Children, Boston, MA, USA.

[6]William G. Lowrie Department of Chemical and Biomolecular Engineering, The Ohio State University, Columbus, OH, USA.

[7]Institute for Experimental Immunology and Imaging, University Hospital, University Duisburg-Essen, Essen, Germany.

[8]Leibniz-Institut für Analytische Wissenschaften–ISAS–e.V., Dortmund, Germany.

[9]Bioinformatics and Molecular Genetics, Faculty of Biology, Centre for Biochemistry and Molecular Cell Research, Faculty of Medicine, Signalling Research Centres BIOSS and CIBSS, University of Freiburg, Freiburg, Germany.

[10]Division of Rheumatology and Immunology, Department of Medicine, Duke University School of Medicine, Durham, NC, USA.

[11]Laboratory of Immune System Biology, National Institute of Allergy and Infectious Diseases, Bethesda, MD, USA.

[*]**Corresponding author.** laemmermann@ie-freiburg.mpg.de.

**Author contributions**: K.Ki. and K.M.G.: conceptualization, investigation, methodology, validation, formal analysis, visualization, and writing review and editing; K.M.G.: software; S.E. and K.Kn.: investigation and methodology; M.M. and M.W.E.: investigation; M.G., R.B., T.K.T.: resources; R.N.G.: writing review and editing; E.R. and D.I.: resources, methodology; W.K.: methodology and writing review and editing; T.L.: conceptualization, funding acquisition, project administration, supervision, investigation, formal analysis, methodology, visualization, writing original draft; ICMJE guidelines were taken into consideration.

**Competing interests:** The authors declare no competing interests.

**Data and materials availability:** All data are available in the main text or the supplementary materials. The use of *Grk3*-deficient mice was restricted by a material transfer agreement with Duke University. The source code for generating displacement–time plots is available at: https://github.com/KMGlaser/Kienle-et-al.git (66).

## Abstract

Neutrophils communicate with each other to form swarms in infected organs. Coordination of this population response is critical for the elimination of bacteria and fungi. Using transgenic mice, we found that neutrophils have evolved an intrinsic mechanism to self-limit swarming and avoid uncontrolled aggregation during inflammation. G protein–coupled receptor (GPCR) desensitization acts as a negative feedback control to stop migration of neutrophils when they sense high concentrations of self-secreted attractants that initially amplify swarming. Interference with this process allows neutrophils to scan larger tissue areas for microbes. Unexpectedly, this does not benefit bacterial clearance as containment of proliferating bacteria by neutrophil clusters becomes impeded. Our data reveal how autosignaling stops self-organized swarming behavior and how the finely tuned balance of neutrophil chemotaxis and arrest counteracts bacterial escape.


## Graphical Abstract

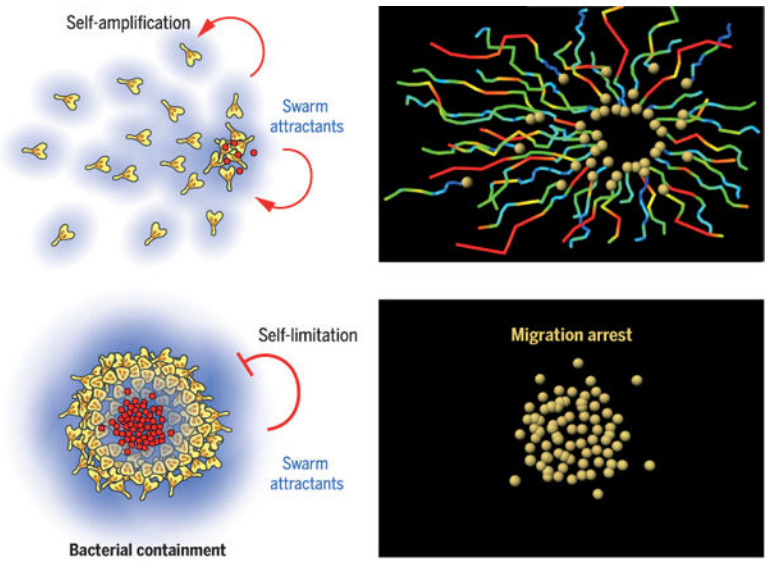


**Self-organization of neutrophil swarms.** Top: Swarming neutrophils self-amplify their highly chemotactic recruitment toward sites of tissue injury or bacterial invasion by releasing attractants that act on neighboring neutrophils. Neutrophils are displayed as spheres with migration tracks (right). Bottom: The local accumulation of the same cell-secreted attractants stops neutrophils when they accumulate and form clusters, a process important for the containment of bacteria in infected tissues.

## Research Summary

**INTRODUCTION:** The collective behavior of cells and insects often relies on self-organizing processes. By releasing attractant signals, a few individuals can initiate the accumulation and aggregation of a whole population. Neutrophils, key players in the innate immune response, infiltrate inflamed and infected tissues in large numbers. These cells make use of such positive feedback amplification to find and kill bacteria in tissues. By secreting attractants that act through cell surface–expressed G protein–coupled receptors (GPCRs) on neighboring cells, neutrophils use this form of intercellular communication and coordinate their hunt for pathogens as a swarm. How

this swarming response is terminated to avoid uncontrolled neutrophil accumulations and prevent excessive inflammation is currently unknown.

**RATIONALE:** The stop signals for neutrophil swarming in mammalian tissues have not yet been defined. They may be derived from cells of the surrounding inflammatory environment or from neutrophils themselves. We reasoned that the attractants released by neutrophils may become highly concentrated at sites where these cells cluster in larger numbers. It is well established that high chemoattractant concentrations can attenuate cellular responses by a process termed GPCR desensitization. We hypothesized a self-limiting mechanism for swarming: The local accumulation of the same neutrophil-expressed attractants that amplify swarming during early stages would cause desensitization of their respective GPCRs at later stages of neutrophil clustering. This led us to investigate the role of GPCR desensitization in neutrophil tissue navigation and host defense.

**RESULTS:** We generated mouse strains whose neutrophils were deficient in GPCR kinases (GRKs), critical enzymes for mediating the GPCR desensitization process. Of the four GRK isoforms tested, in vitro experiments identified GRK2 as the kinase necessary to desensitize GPCRs activated by swarm-released attractants (LTB4 and CXCL2). When neutrophils sense high concentrations of swarm attractants in vitro, GRK2 desensitizes the corresponding receptors to induce migration arrest. Two-photon intravital imaging of injured skin and infected lymph nodes of mice showed that GRK2 and GPCR desensitization play critical roles during neutrophil swarming in physiological tissue. At sites where swarming neutrophils accumulate and self-generate local fields of high swarm attractant concentration, GPCR desensitization was crucial to stop neutrophil migration arrest. Desensitization-resistant neutrophils moved faster and explored larger areas of lymph node tissue infected with the bacterium *Pseudomonas aeruginosa*. Such behavior suggested more effective bacterial sampling throughout the infected organ. Surprisingly, mice with GRK2-deficient neutrophils showed impaired rather than improved bacterial clearance. This finding could not be explained by altered antibacterial effector functions. In vitro assays for the detailed analysis of swarming behavior and bacterial growth revealed that GPCR desensitization to swarm attractants is required to induce neutrophil arrest for optimal bacterial phagocytosis and containment in swarm clusters.

**CONCLUSION:** We describe a cell-intrinsic stop mechanism for the self-organization of neutrophil collectives in infected tissues, which is based on sensing the local accumulation of the same cell-secreted attractants that amplify swarming during early stages. GPCR desensitization acts as a negative feedback control mechanism to stop neutrophil migration in swarm aggregates. This navigation mechanism allows neutrophils to self-limit their dynamics within forming swarms and ensures optimal elimination of bacteria. Desensitization to a self-produced activation signal as a principle of self-organization is important for immune host defense against bacteria, and likely informs other categories of collective behavior in cells and insects.

The collective behavior of eukaryotic cells and insects is often based on self-organizing processes. The release of chemical signals, such as chemoattractants or pheromones, is one mechanism that allows individual entities to attract neighboring individuals, leading to the accumulation and aggregation of a whole population of cells or insects. Examples of such self-amplifying positive feedback control to initiate phases of self-organization include the collective defensive behavior of honey bees that attack hornets by thermo-balling (1), the aggregation behavior of locusts (2), and signal relay during the life cycle of *Dictyostelium*

(3). However, the mechanisms that stop self-organization are poorly understood for many of these processes.

Neutrophils circulate in large numbers in the mammalian bloodstream to patrol the body, thereby playing a central role in host defense (4). They exit blood vessels and infiltrate tissues to search for damaged cells and invading pathogens when local surveillance by other tissue-resident immune cells fails to control inflammation or infection (5, 6). Therefore, neutrophil infiltrates and aggregates represent major histopathological hallmarks of acute tissue inflammation and infection. Intravital imaging in mouse tissues has revealed that collective-like swarming behavior underlies the formation of neutrophil aggregates in many mouse models of sterile tissue injury and infection with bacteria, fungi, and viruses (7, 8). During this population response, hundreds of individual neutrophils show coordinated sequential phases of highly directed chemotaxis, intercellular signal relay, and cluster formation. Reminiscent of the collective behavior of some insects and *Dictyostelium*, neutrophils self-amplify swarming in a feedforward manner by secreting chemokines and chemoattractants, which allows intercellular communication and provides the swarm with a level of self-organization in the complexity of an inflammatory environment (9).

It remains unclear how this swarming response ceases and thereby avoids uncontrolled neutrophil accumulation. The mechanisms for terminating this response in mammalian tissues have not yet been defined and may be controlled by external factors from the tissue environment or by neutrophils themselves, as suggested from simpler model systems (10–12). On the basis of our previous findings that neutrophils self-amplify swarming through the release of the chemoattractants LTB4 (leukotriene B4) and CXCL2 (chemokine C-X-C motif chemokine ligand 2) (9), we hypothesized that the temporal local increase of these attractants causes the desensitization of the respective G protein–coupled receptors (GPCRs) (13), potentially acting as an internal feedback control for swarming neutrophils. It is well established that neutrophils can undergo GPCR desensitization and become unresponsive to repeated or continuous agonist stimulation in vitro (14–16). However, it remains unresolved whether and how this process contributes to neutrophil navigation and swarming in mammalian tissues, or whether the anticipated desensitization plays a role in their physiological host defense functions.

## GRK2 controls GPCR desensitization and neutrophil arrest

We began our study of these issues by first examining whether active desensitization occurs during swarming. To this end, we interfered with GPCR desensitization by genetically targeting GPCR kinases (GRKs). These critical enzymes can phosphorylate cytoplasmic tails of an activated GPCR, which ultimately leads to the uncoupling of the GPCR from its signaling cascade and often GPCR internalization as well (13) (fig. S1A). Because neutrophils express four GRK isoforms (GRK2, GRK3, GRK5, and GRK6) (17–21), we crossed several mouse strains to isolate primary mature neutrophils that were efficiently depleted of individual GRKs or the complete GRK family (fig. S1, B to E). To identify the GRK isoforms that are functionally relevant for swarming, we imaged control and *Grk*-deficient neutrophils side-by-side in chemotaxis assays and analyzed their migratory response toward gradients of the primary swarm-mediating attractants LTB4 and CXCL2

(Fig. 1A). In these experiments, control neutrophils performed highly directed chemotaxis at the onset of the gradient before they slowed down, rounded up, and stopped migrating when reaching areas of high attractant concentrations (Fig. 1,B to D, fig. S1F, and Movie 1).

Among all single *Grk*-deficient cells, only neutrophils lacking GRK2 (*Grk2*$^{-/-}$) displayed clearly distinct behavior. Previous work has shown that GRK2 in B and T cells selectively controls the desensitization of the GPCR sphingosine-1-phosphate receptor 1 (S1PR1), but not of several other lymphocyte-expressed GPCRs (22). In gradients of combined LTB4 and CXCL2, *Grk2*$^{-/-}$ neutrophils showed twice the displacement of control cells from the starting cell well (Fig. 1, A and B, and Movie 1). Maximum displacement of knockout cells ranged from 1.7 to 3.2 mm between independent experiments, whereas control cells reached 1 to 1.5 mm. At the onset of the gradient (early phase, 0 to 30 min), *Grk2*$^{-/-}$ neutrophils showed a slight increase in speed and *y*-straightness, a measure of chemotactic behavior, in comparison to control cells (Fig. 1C). However, the major effect of GRK2 depletion was observed in fields of high attractant concentrations (late phase, 90 to 180 min). *Grk2*$^{-/-}$ neutrophils did not arrest as did control cells, but they continued to move with polarized morphology at elevated speed (Fig. 1, D and E), before reaching an oscillating behavior with short alternating phases of forward and backward movement (fig. S1G). Similar motility behavior was observed in single gradients of LTB4 and CXCL2 alone (Fig. 1, F and G, and fig. S1G). We never observed net reverse migration of *Grk2*$^{-/-}$ cells. This persistent migration phenotype could not be attributed to gross alterations in the differentiation and maturation of control and *Grk2*$^{-/-}$ bone marrow neutrophils (fig. S2A). Notably, the same GRK2 dependency was also evident with neutrophils isolated from blood (fig. S2, B and C), preactivated neutrophils (fig. S2D), and wild-type neutrophils upon acute chemical GRK2 inhibition (fig. S2E). Depletion of all four GRK isoforms in neutrophils (4×*Grk*$^{-/-}$) did not additionally increase the migratory response in LTB4/CXCL2 gradients (Fig. 1A, fig. S2F, and Movie 1), highlighting the major role of GRK2 in this process.

*Grk2*$^{-/-}$ neutrophils did not show this substantial increase in responsiveness for all GPCR ligands known to attract neutrophils. When comparing the displacement of *Grk2*$^{-/-}$ relative to control neutrophils in gradients of attractants binding to formyl peptide receptors (FPR1 and FPR2) or the complement component 5a anaphylatoxin chemotactic receptor 1 (C5aR1), which are GPCRs that do not show an important role during neutrophil swarming to modest sterile injury (9), we could only measure minimal or statistically nonsignificant differences (Fig. 1F). These findings indicated a particular role for GRK2 in controlling GPCRs that sense neutrophil-secreted LTB4 and CXCL2 and contribute to the self-amplification of neutrophil swarming. Because GRK2 can also act on non-GPCR substrates (23), we directly tested GPCR desensitization by exposing neutrophils to repeated stimulation with increasing concentrations of agonist and measured the transient increase in intracellular calcium as a readout for cellular responsiveness. Control neutrophils became unresponsive upon sequential stimulation, whereas *Grk2*$^{-/-}$ neutrophils remained responsive to a third GPCR activation through LTB4 or CXCL2 (Fig. 1, H and I). As a consequence, *Grk2*$^{-/-}$ neutrophils showed increased activation of promigratory mitogen-activated protein kinase (MAPK) signaling cascades downstream of GPCR activation when we activated cells with the same triple rising stimulation that was used in the calcium flux assay (fig. S3, A and B). Notably, repeated stimulation of control and *Grk2*$^{-/-}$ neutrophils with the attractant

complement component 5a (C5a) did not produce any differences in calcium and MAPK signaling measurements (fig. S3C). To test the effect of GPCR desensitization on neutrophil movement, we pretreated control and *Grk2*$^{-/-}$ cells with concentrations of LTB4 and CXCL2 that caused receptor desensitization in the calcium flux assay, before analyzing GPCR-mediated chemokinesis. In agreement with our results on GPCR desensitization in calcium and MAPK signaling measurements, ligand-pretreated *Grk2*$^{-/-}$ cells were more chemokinetic than control cells for both LTB4 (fig. S3D) and CXCL2 (fig. S3, E and F), as reflected by increased speed and track lengths.

Lastly, we tested whether GRK2-controlled desensitization is accompanied by receptor internalization. In agreement with previous reports that found little if any internalization of the LTB4 receptor 1 (LTB4R1) (24–26), we did not observe any reduction in cell surface expression of this receptor in wild-type and *Grk2*$^{-/-}$ cells upon exposure to high concentrations of LTB4 (fig. S3G). There was a time-dependent decrease in cell surface expression of the C-X-C motif chemokine receptor 2 (CXCR2) in both wild-type and *Grk2*$^{-/-}$ neutrophils, in agreement with previous reports (26). However, cell surface levels of CXCR2 remained substantially higher in *Grk2*$^{-/-}$ neutrophils (fig. S3H). Thus, GRK2 plays a crucial role in attenuating GPCR activation with swarm-mediating attractants, which maintains neutrophil motility in fields of high attractant concentrations.

## Neutrophils and eosinophils self-limit swarming

Neutrophil swarms come in a range of phenotypes and can be categorized into persistent and transient swarms (7). Persistent swarms show sustained neutrophil recruitment to form large cell clusters that can remain stable for hours, whereas transient swarms form smaller clusters that last only for minutes before neutrophils leave the aggregate and join nearby competing swarms. To investigate the role of GPCR desensitization for persistent swarm dynamics, we first used large microscale arrays of fluorescent heat-killed bioparticle clusters, a previously established experimental system to analyze neutrophil swarming in vitro (12). Upon exposure to 400 μm–spaced micropatterns of heat-killed *Staphylococcus aureus* (HKSA), sentinel neutrophils sensed the bioparticles and induced a recruitment wave of following neutrophils, which then formed cell clusters in a LTB4- and CXCL2-dependent manner (12) (Fig. 2A and fig. S4, A and B). In experiments with 1:1 mixtures of differentially dye-labeled control and *Grk2*$^{-/-}$ cells, we quantified neutrophil aggregation behavior in competitive clusters (fig. S4C). The accumulation index (AI), which is the ratio of *Grk2*$^{-/-}$ signal to wild-type signal on HKSA spots, was used as a measure of neutrophil aggregation. Strikingly, *Grk2*$^{-/-}$ neutrophils showed pronounced aggregation and dominated over control cells in competitive clusters—a behavior that was reflected in a mean AI value greater than 1 (Fig. 2B and fig. S4C). By comparison, competitive clusters of two populations of control cells resulted in a mean AI of 1 (Fig. 2B).

Next, we examined the role of GRK2 in regulating persistent swarms in vivo by using an inducible model of sterile skin injury in which a brief laser pulse causes focal, dermis-restricted tissue damage (9). After intradermal (i.d.) co-injection of differentially dye-labeled control and *Grk2*$^{-/-}$ neutrophils, we used two-photon intravital microscopy (2P-IVM) to image the swarming response of the transferred cells to the induced skin wound for 1 to 1.5

hours (Fig. 2C and fig. S5A). Neutrophils that swarmed from the surrounding tissue toward the site of injury were tracked and migration parameters analyzed (Fig. 2D and fig. S5B). Control and *Grk2*$^{-/-}$ neutrophils were recruited at comparable speed and straightness toward the injury site (Fig. 2E, fig. S5C, and Movie 2), demonstrating that the minor measured effect on early-phase chemotaxis in vitro was not relevant for migration in native tissue (Fig. 1C).

We then analyzed the ensuing step of the swarming response, swarm aggregation. To quantify neutrophil clustering in the skin, we defined the AI as a measure of cell entry into the collagen-free zone, as previously described (9). In (9), we only identified gene knockouts that showed impaired neutrophil aggregation behavior and mean AI values less than 1. Remarkably, *Grk2*$^{-/-}$ neutrophils gravitated more than wild-type cells toward the central region of large competitive clusters, resulting in mean AI values less than 1 (Fig. 2, F to H, and fig. S5D). Improved aggregation behavior of *Grk2*$^{-/-}$ cells was also observed in experimental setups that allowed the analysis of small clusters (fig. S5E and Movie 2). In contrast to control cells, *Grk2*$^{-/-}$ neutrophils remained actively motile in a growing cluster and continued to move toward the cluster center, where they outcompeted wild-type cells over time (Fig. 2G, fig. S5D, and Movie 2). GRK3, GRK5, or GRK6 deficiency had no measurable effect on central accumulation (Fig. 2H and fig. S5F).

Finally, we studied persistent swarms of eosinophils, another innate immune cell type, that self-amplify their collective migration response to worms by paracrine LTB4 signaling (27). Like neutrophils, swarming *Grk2*$^{-/-}$ eosinophils aggregated more closely than wild-type cells around *C. elegans* larvae (Fig. 2I, fig. S5G, and Movie 2), confirming the more general role for GRK2 in swarming responses beyond neutrophil biology. Thus, GRK2 acts as negative regulator of swarming in mammalian tissues, and GPCR desensitization is integral at sites where swarming granulocytes accumulate and self-generate a local field of high attractant concentrations.

## Increased tissue scanning is not beneficial for bacterial elimination

In many inflammatory conditions, neutrophils respond to cell death at multiple locations within a tissue, leading to several transient swarms whose attractant release influences each other’s growth and disappearance (7). To address the role of GRK2 in situations where migrating neutrophils sense multiple attractant sources, we preexposed wild-type and *Grk2*$^{-/-}$ neutrophils to LTB4/CXCL2 before they moved along a gradient of both agonists. In agreement with our calcium measurements (Fig. 1, H and I), wild-type neutrophils desensitized and became unresponsive to the subsequent attractant gradient in a concentration-dependent manner. By contrast, *Grk2*$^{-/-}$ neutrophils remained responsive at high attractant concentrations and could still move along the gradient of activating signals (fig. S6A).

Next, we analyzed the sequential navigation behavior of neutrophils in the presence of two spatiotemporally separated gradients of swarm attractants (Fig. 3A) (28). As observed previously (Fig. 1, A to D), *Grk2*$^{-/-}$ neutrophils showed increased displacement from a starting cell well toward an initial source of LTB4/CXCL2 in comparison to control cells.

*Grk2*$^{-/-}$ neutrophils were redirected by an additional second gradient at 90° angle, whereas control cells were not (Fig. 3A, fig. S6, B and C, and Movie 3). Thus, neutrophils lacking GRK2-mediated GPCR desensitization increase their space exploration between competing gradients of swarm attractants.

To gain insight into the possible in vivo relevance of our findings, we investigated the role of GRK2 during transient neutrophil swarming in lymph nodes infected with *Pseudomonas aeruginosa* or *Salmonella typhimurium*. We previously showed that several bacteria species induce cell death in subcapsular sinus (SCS) macrophages, subsequently leading to neutrophil recruitment and swarming in lymph nodes (9, 29) (Fig. 3B). Neutrophil depletion in these infection models leads to a substantial increase of bacteria growth in lymph nodes (29). By imaging endogenous wild-type and *Grk2*$^{-/-}$ neutrophils in SCS of mixed bone marrow chimera, we found again that knockout cells dominated over control cells in the central regions of newly forming clusters (Fig. 3, C and D, fig. S6, D and E, and Movie 3). This was reflected in AI values less than 1 (Fig. 3D). Moreover, *Grk2*$^{-/-}$ neutrophils moved faster than wild-type cells between clusters and explored larger tissue areas (Fig. 3E, fig. S6F, and Movie 3). Such behavior may be linked to more effective bacterial sampling throughout the infected organ, leading us to undertake a quantitative assessment of how GRK2 deficiency in neutrophils affects bacterial clearance. The draining lymph nodes of mice with neutrophilspecific depletion of GRK2 (*Mrp8Cre Grk2*$^{fl/fl}$, "*Grk2*$^{\Delta PMN}$") and controls were analyzed after subcutaneous (s.c.) infection with *P. aeruginosa*. To our surprise, there were significantly higher bacterial counts in the lymph nodes of *Grk2*$^{\Delta PMN}$ mice relative to control mice (Fig. 3F), although neutrophil recruitment into infected lymph nodes was comparable (fig. S6G). Thus, an inverse relationship exists between persistent neutrophil interstitial movement and bacterial elimination.

## GPCR-controlled neutrophil arrest is critical for restricting bacterial growth

To understand in detail how GRK2-controlled neutrophil swarming counteracts bacterial growth, we established an experimental in vitro mimic of a bacteria-infected SCS. By coculturing macrophages, neutrophils, and *P. aeruginosa* bacteria, we were able to follow the dynamics and major cellular events of SCS components with live-cell microscopy (Fig. 4A). In this system, bacteria performed pack swarming and invasion of macrophages (30), causing cell death as previously shown in vivo (29) (fig. S7, A to C, and Movie 4). Neutrophils showed swarming behavior and formed prominent clusters around locally proliferating bacteria and dying cells (Fig. 4B and fig. S7D). In agreement with our in vivo findings, *Grk2*$^{-/-}$ neutrophils dominated over control cells in cluster centers in competitive experiments (fig. S7E). When control and knockout cells were studied individually, *Grk2*$^{-/-}$ cells formed larger neutrophil aggregates around bacterial clusters than did wild-type cells (Fig. 4C and Movie 4). However, GRK2 deficiency resulted in higher counts of "free" bacteria outside of neutrophil clusters and a significant increase of bacterial growth (Fig. 4C), confirming the results of our mouse infection model. This could not be attributed to changes in neutrophil maturation or major effector functions, as *Grk2*$^{-/-}$ and control cells were comparable in standard phagocytosis assays (HKSA and living *P. aeruginosa*) and in their release of reactive oxygen species, neutrophil elastase, and myeloperoxidase (fig. S8, A to E). We also only rarely observed neutrophil extracellular traps (NETs) around the

small bacteria aggregates in our coculture system and depletion of GRK2 had no measurable effect on NET formation (fig. S8F), a process that has previously been reported to occur in the presence of *P. aeruginosa* biofilms (31). Establishing single-cell tracking of neutrophils in clusters helped us to identify the GRK2-regulated cellular mechanism limiting bacterial growth. Control cells slowed down their persistent migration and stopped in cell aggregates, whereas many *Grk2*$^{-/-}$ neutrophils lacked such arrest phases and migrated at high speed out of clusters again (Fig. 4, D to F, fig. S7F, and Movie 4).

This uncontrolled persistent movement of *Grk2*$^{-/-}$ neutrophils had two functional consequences. First, knockout cells were impaired in picking up and ingesting microbes from bacteria clusters (Fig. 4G). Second, *Grk2*$^{-/-}$ cells were often unable to completely contain locally proliferating bacteria, allowing a breach in the swarm-dependent barrier and subsequent pathogen escape (Fig. 4H). Thus, GRK2-controlled neutrophil arrest is critical for bacterial phagocytosis and containment in swarm clusters. These findings emphasize that neutrophils have evolved a cell-intrinsic mechanism that self-limits dynamic cell behavior within forming swarms and ensures optimal elimination of bacteria (figs. S9 and S10).

## Discussion

Neutrophil navigation through inflamed and infected tissues has long been viewed from a single-cell perspective, where cells were considered to be individually guided by external signals released from the tissue environment or directly from pathogens. It is now clear that neutrophils autosignal to initiate a self-amplified population response, which accumulates these cells in large numbers and concentrates their effector functions at sites of damaged tissue or pathogen invasion (7, 9). We have described a cell-intrinsic stop mechanism for the self-organization of collective behavior, which is based on sensing the local accumulation of the same cell-secreted attractants that amplify swarming during early stages. Our findings highlight a crucial role of GPCR desensitization in attenuating the self-organized swarming dynamics of neutrophils in mammalian tissues (fig. S9). When neutrophils sense high concentrations of swarm-secreted attractants (LTB4 and CXCL2), as found in growing neutrophil clusters, the GPCR kinase GRK2 desensitizes the corresponding GPCRs to induce migration arrest. Because GRK2 has only minimal effects on the desensitization of GPCRs that detect tissue- or bacteria-derived attractants (e.g., N-formyl peptides and C5a), neutrophils in swarm aggregates remain responsive to new tissue insults. This allows their redirection from neutrophil clusters to novel sites of cell death in tissues. Thus, our findings agree with earlier in vitro studies that highlighted the capacity of “end-target” attractants (N-formyl peptides and C5a) to override “intermediary” attractants (LTB4, CXCL2) and redirect neutrophils out of “intermediary” attractant fields (28, 32). The described GRK2-mediated feedback control to swarm attractants is particularly critical in infected tissues, where it fine-tunes the local migratory arrest of neutrophils for optimal containment of proliferating bacteria (fig. S10). This provides a potential mechanistic explanation for earlier studies that implicated neutrophil swarming in restricting microbial growth in vitro (33) and in vivo (34). Although we identified GRK2 as a key molecular brake on GPCR activation by neutrophil swarm attractants, its function may extend to other GPCRs in different inflammatory settings (35, 36).

How migrating phagocytes coordinate cell movement and phagocytosis and negotiate these two actin-dependent processes has been intensely studied in other phagocytic cells, including dendritic cells, *Dictyostelium*, and *Drosophila* macrophages (37–43). Most of these studies were performed in vitro or in simpler model organisms and focused on the analysis of individual cells and their uptake of inert elements. By contrast, we have addressed the population dynamics of phagocytes and how these cells coordinate stop-and-go behavior within the population by self-secreting attractants. We define a cell-intrinsic, GPCR-based mechanism for stopping the swarming behavior of neutrophils, which is functionally relevant for the containment of proliferating living bacteria in infected mammalian tissues. This self-limiting mechanism does not rely on adaptations in gene regulation, as commonly found in the bacterial population responses of quorum sensing and quenching (44). Local attractant degradation and the release of pro-resolving mediators are other potential self-limiting processes that emerged from in vitro studies (12, 45). However, it is still unclear whether these processes also contribute to neutrophil swarming in tissues and augment the mechanism described herein.

These findings provide insights into the navigation strategies used by neutrophil populations for the optimal elimination of bacteria in infected mammalian tissues. This should prove useful for an integrated view of self-limiting processes and active anti-inflammatory programs in controlling the resolution of neutrophil swarms, which is a critical step for tissue repair after infection. Our results also highlight the fact that desensitization to a self-produced activation signal acts as an important biological principle of self-organization, which is likely relevant for other forms of collective behavior in cells and insects.

## Materials and methods

### Mice

Table S1 lists all mouse strains and crosses used in this study. *Mrp8-Cre* (46), $Grk2^{fl/fl}$ (47), $Grk3^{-/-}$ (48), $Grk5^{fl/fl}$ (49), $Grk6^{fl/fl}$ (50), $Lyz2^{gfp}$ (51), $Ly6g^{cre/+}$ $Rosa26^{LSL:Tom}$ (52), *Vav-iCre* (53), *CAG-DsRed* (54), $Tyr^{c\text{-}2J/c\text{-}2J}$ (B6.Albino) (55, 56), and Lifeact-GFP (57) mouse strains have been described elsewhere. Mice were maintained in specific pathogen–free conditions at an Association for Assessment and Accreditation of Laboratory Animal Care–accredited animal facility at NIAID and in a conventional animal facility at the Max Planck Institute of Immunobiology and Epigenetics according to local regulations. Mice were used for experiments at 8 to 16 weeks of age. Mice were age- and sex-matched in all experiments, and littermate animals were used as controls in most experiments. All animal procedures were performed according to study protocols approved by the German authorities and the Regional Council of Freiburg, the Animal Care Commission of the state of North Rhine–Westphalia (LUA NRW), and the NIAID Animal Care and Use Committee, respectively.

### Neutrophil isolation and labeling

For all in vitro experiments, mouse neutrophils were isolated from bone marrow (tibiae, femora, and os coxae) or peripheral blood using autoMACS Pro Selector cell separator and MACS Neutrophil Isolation Kit for negative selection according to the manufacturer's

protocol (Miltenyi Biotec). For i.d. injection experiments, mouse neutrophils were isolated from bone marrow using a three-layer Percoll gradient of 78%, 69%, and 52% as described (9). Neutrophil purity was >95% for both isolation procedures, as indicated by $Ly6G^+$ phenotype in flow cytometry. When neutrophils required fluorescent cell labeling in subsequent experiments, they were incubated for 25 min at $2 \times 10^7$ cells/ml with 0.5 μM CellTracker Green (CMFDA), 10 μM CellTracker Blue ($CMF_2HC$), 1 μM CellTracker Deep Red, or 10 μM 5-carboxytetramethylrhodamine, succinimidyl ester (5-TAMRA SE) in 1× PBS supplemented with 0.0002% (w/v) pluronic F-127 (all Thermo Fisher), as indicated for each experiment. After labeling, neutrophils were washed three times with 2% fetal bovine serum (FBS) and 2 mM EDTA in HBSS. In most experiments, neutrophils isolated from bone marrow were used, if not otherwise indicated.

## Neutrophil chemotaxis and navigation assays

To analyze GPCR-driven neutrophil migration toward increasing concentrations of chemoattractants, we used under-agarose chemotaxis assays with slight modifications to the standard protocol (58). Agarose gels were cast into 35 × 10-mm tissue culture dishes (Corning). After gel polymerization, wells with a diameter of 4 mm were punched into the gel in ~3-mm distances using a template. Unless stated otherwise, five wells were punched in the agarose gel per dish: one central well for the chemoattractant surrounded by four equidistant wells for the cells. For side-by-side comparisons of control and gene-deficient neutrophils, cells were differentially labeled with CellTracker Green and 5-TAMRA SE. Neutrophils isolated from a pair of GRK-deficient and control mice were used for an independent experiment. Four technical replicates were performed in one independent experiment: two replicates with one dye combination, the other two replicates with interchanged dyes between control and gene-deficient neutrophils to exclude unspecific effects. Data analysis is described below. For triple comparisons of wild-type, $Grk2^{-/-}$, and $4\times Grk^{-/-}$ neutrophils, the third neutrophil population was labeled with CellTracker Blue. The outer four wells in the agarose gel were loaded with 20 μl of control and GRK-deficient neutrophils at a ratio of 1:1 (double comparison) or 1:1:1 (triple comparison) to obtain $10^5$ cells in 10% FBS and 2 mM L-glutamine in phenolfree RPMI. The central well was loaded with 20 μl of chemoattractant at the following concentrations, if not indicated otherwise: 1 μM LTB4 (Cayman) and 1 μM murine CXCL2 (PeproTech), 1 μM LTB4 alone, 1 μM murine CXCL2 alone, 10 μM WKYMVM (Tocris), 1 μM WKYMVm (Tocris), or 1 μM murine C5a (PeproTech). For chemotaxis experiments referred to as “FPR1 stim,” the FPR1/FPR2 selective chemoattractant WKYMVm was used in the presence of the selective FPR2 inhibitor WRW4 (100 μM, Tocris). Experiments with the selective FPR2 chemoattractant WKYMVM were referred to as “FPR2 stim.” To acutely inhibit GRK2 function in control neutrophils, cell chemotaxis was performed in the presence of 30 μM CMPD101 (HelloBio). For every inhibitor treatment, cells were first pre-incubated with the inhibitor for 30 min at 37°C and then directly transferred to the wells without inhibitor washout. For neutrophil preactivation, TNF-α (50 ng/ml) was added to the cells for 10 min before loading. To mimic the activation that neutrophils undergo upon extravasation into an inflamed tissue (59), cells were pre-incubated in a Lab-Tek (Thermo Fisher/Nunc) coated with murine CXCL1 (KC) (10 μg/ml; PeproTech), ICAM-1 (8 μg/ml; R&D Systems), and PECAM-1 (2 μg/ml; R&D Systems) for 1 hour before transfer to the chemotaxis dish. To analyze

sequential navigation behavior, neutrophils were exposed to a first gradient of LTB4/CXCL2 (0.5 μM each), before adding 3 hours later a second gradient of LTB4/CXCL2 (1 μM each) at a 90° angle. For pre-incubation experiments, neutrophils were pre-incubated with LTB4/CXCL2 (0.1 μM or 1 μM each) for 30 min before chemoattractants were washed out and cells subsequently loaded into the wells of the under-agarose assay. Neutrophil migration was followed for 4 hours at 37°C. Cells that migrated along the chemoattractant gradient underneath the agarose gel were recorded. Images were acquired for each well with a spinning-disk confocal microscope (Carl Zeiss Microimaging) at 10× magnification using multiple tiles to capture the whole well including all cells that left the well. Live-video microscopy was performed using a confocal spinning-disk microscope equipped with a stage-top incubator (Tokai-Hit) to generate an ambient atmosphere of 37°C and 5% $CO_2$. For confocal spinning-disk microscopy, we used a Cell Observer SD system (Carl Zeiss) comprising a CSU-X1 confocal scanner unit (Yokogawa) mounted on an AxioObserver Z1 inverted microscope stand, and equipped with Evolve back-illuminated EM-CCD camera (Teledyne Photometrics). Depending on the used fluorochromes, images were acquired using laser-line excitation by 488-nm, 561-nm, 405-nm, or 639-nm solid-state lasers. A Plan-Apochromat 10× 0.45 objective and multiple-tiles function in ZEN software were used for image acquisition during live-cell imaging experiments and for experiments with endpoint analysis.

### Neutrophil swarming on micropatterns

Microscale arrays of bioparticle clusters were manufactured as described (12). For pattern design, heat-killed *S. aureus* (SA) Texas Red particle conjugates (Sigma-Aldrich) were used. The slides had an eight-well table format consisting of 10 patterns per row arranged in eight columns with single pattern diameters of 130 μm. Before neutrophils were added, wells were coated with 10% SA-opsonization reagent (Thermo Fisher Scientific) and fibronectin (10 μg/ml) in FBS for 1 hour followed by three washes with 1× PBS. Control and GRK2-depleted neutrophils were differentially labeled with CellTracker Green and 5-TAMRA SE, mixed 1:1 and preactivated with TNF-$\alpha$ (50 ng/ml; PeproTech) for 10 min. Neutrophils were then suspended in bovine collagen I (Nutacon) at a final gel concentration of 1 mg/ml and a density of $2 \times 10^6$ cells/ml, before 180 μl of the neutrophil-gel suspension was added to each well. To inhibit leukotriene biosynthesis, neutrophils were pre-incubated with 10 μM MK-886 (5-lipoxygenase-activating protein inhibitor, Calbiochem) for 30 min. To inhibit CXCL2 signaling, neutrophils were pre-incubated with 50 μM SB225002 (CXCR2 antagonist, Tocris) for 30 min. Loaded slides were incubated for 2 to 3 hours at 37°C before image acquisition. Images of whole slides were acquired at 10× magnification using the confocal spinning-disk microscope system as described above.

### Eosinophil swarming assay

Eosinophils were obtained from a murine bone marrow culture according to a reported protocol (60). In brief, cultures of bone marrow cells were first supplemented with SCF (100 ng/ml) and FLT3-L (100 ng/ml; PeproTech) for 4 days. On day 4, the medium was replaced with medium containing murine IL-5 (10 ng/ml; PeproTech). Every second day, one-half of the medium was replaced by medium containing fresh IL-5 until eosinophils were ready to use on day 14. Eosinophil maturation was checked by Siglec-F expression using flow

cytometry (>99% Siglec-F$^+$ cells at day 14). Bone marrow of *Vav-iCre Grk2$^{fl/fl}$* mice was used to deplete GRK2 in eosinophils. Four-day-old *C. elegans* dauer larvae carrying the *daf-2 (e1370)* allele were prepared by growing the worms at 25°C using standard methods, and kindly provided by R. Baumeister (University of Freiburg, Germany). Eosinophil swarming in response to nematodes in a 3D in vitro system has been described (27). Briefly, nematodes were suspended at a concentration of 6000 larvae/ml in Matrigel (Corning). Control and fgene-deficient eosinophils were differentially labeled with CellTracker Green and 5-TAMRA SE, and mixed 1:1 at a concentration of $3 \times 10^6$ cells/ml. Eosinophils in medium were mixed with nematodes in Matrigel at a 1:1 ratio and added into eight-well Lab-Tek imaging chambers. After 2 hours of incubation, images of single nematodes were acquired. Live-video microscopy was performed using a spinning-disk confocal microscope equipped with a stage-top incubator to generate an ambient atmosphere of 37°C and 5% $CO_2$. For time-lapse videos, an LD LCI Plan-Apochromat 25×/0.8 objective (Zeiss) was used and images were acquired every minute for 2 hours. For quantitative analysis, single images of individual nematodes with clusters of eosinophils were acquired after 2 hours at 10× magnification using the confocal spinning-disk microscope system as described above.

### Neutrophil GPCR desensitization: Calcium flux analysis

To analyze GPCR desensitization in response to increasing concentration of chemoattractant, transient increases of intracellular calcium ($Ca^{2+}$) in neutrophils were measured by flow cytometry. Neutrophils isolated from bone marrow were loaded with Indo-1 AM (2 μg/ml) according to the manufacturer's instructions (Thermo Fisher Scientific). In brief, ratiometric changes in intracellular calcium flow were measured using a LSRIII flow cytometer (BD Biosciences) equipped with a sample heater at 37°C. Before acquisition, neutrophils were prewarmed in a water bath at 37°C for 10 min. During acquisition, neutrophils were maintained in a sample heater at 37°C and only removed briefly for stimulant addition. At the beginning of experiments, a 30-s baseline was recorded. Then, cells were stimulated at $t = 0.5$ min, $t = 4$ min, and $t = 8$ min, and real-time intracellular $Ca^{2+}$ flux was recorded. Recording was stopped at $t = 10$ min. Cells were stimulated with increasing concentrations of LTB4 (50 nM, 100 nM, and 200 nM) (Fig. 1H), CXCL2 (50 nM, 100 nM, and 200 nM) (Fig. 1I), CXCL2 (10 nM, 20 nM, and 40 nM) (fig. S3F), or C5a (5 nM, 10 nM, and 20 nM) (fig. S3C). To quantify receptor desensitization upon multiple stimulations, the area under the curve (AUC) (0 to 100 s after each stimulation) of the $Ca^{2+}$ flux was measured using FlowJo software. Desensitization was measured as the ratio of the AUC of the second or third stimulation to the AUC of the first stimulation in each independent experiment. In rare cases, experiments were excluded from analysis when neutrophils did not display detectable calcium signals after attractant stimulation.

### 2P-IVM of neutrophil swarms in ear skin

Two-photon intravital imaging of persistent neutrophil swarming in response to a laser-induced focal skin injury has been described in detail (9). Control and GRK-deficient neutrophils were incubated for 15 min with 1 μM CMFDA and 0.8 μM CellTracker Red (CMPTX), or vice versa, in 1× Hanks' balanced salt solution (HBSS) supplemented with 0.0002% (w/v) pluronic F-127. Neutrophils were washed four times with washing buffer (1×

HBSS, 1% FBS, 2 mM EDTA), before a 1:1 ratio of differentially dye-labeled control and GRK-deficient neutrophils (each >2 × $10^6$ cells) was taken up in 1× PBS at a volume of 15 to 30 μl. A 5-μl neutrophil suspension was then injected i.d. with an insulin syringe (31 GA needle, BD Biosciences) into the ventral side of the ear pinnae of an isoflurane-anesthetized *Tyr*$^{c\text{-}2J/c\text{-}2J}$ recipient mouse. In one experimental set, neutrophils isolated from either *Grk2* $^{fl/fl}$ *Lifeact-GFP*$^{+/-}$ or *Mrp8-Cre Grk2*$^{fl/fl}$ *Lifeact-GFP* $^{+/-}$ mice were injected into *CAG-DsRed*$^{+/+}$ *Tyr*$^{c\text{-}2J/c\text{-}2J}$ recipient mice to study green fluorescent injected neutrophils side by side with endogenous red-fluorescent wild-type neutrophils. Two to three hours after neutrophil injection, mice were again anesthetized using isoflurane (cp-pharma; 2% for induction, 1 to 1.5% for maintenance, vaporized in an 80:20 mixture of oxygen and air) and placed in a lateral recumbent position on a custom-made imaging platform such that the ventral side of the ear pinna rested on a coverslip. A strip of Durapore tape was placed lightly over the ear pinna and affixed to the imaging platform to immobilize the tissue. Anesthetized mice rested in the heated environmental chamber for 30 to 60 min before a first focal skin injury was induced by a focused two-photon laser pulse at an approximate laser intensity of 80 mW (9). At pixel dimensions of 0.14 μm× 0.14 μm, a circular region of interest (diameter 25 to 35 μm) was defined in one focal plane, followed by laser scanning at a pixel dwell time of 0.8 μs for 35 to 50 iterations, depending on the tissue depth of the imaging field of view. The damage was restricted to dermal layers only. Immediately after laser-induced tissue damage, imaging of the neutrophil response was started at typical voxel dimensions of 0.72 μm × 0.72 μm × 2 μm. Images were mainly captured toward the anterior half of the ear pinna where hair follicles are sparse. Images were acquired using an inverted LSM 510 NLO (at NIH) or LSM 780 NLO (at MPI Freiburg) multiphoton microscope (Carl Zeiss Microimaging) enclosed in a custom-built environmental chamber that was maintained at 32°C using heated air. These systems were fitted with at least three external non-descanned photomultiplier tube detectors in the reflected light path. Images were acquired using a 25×/0.8 numerical aperture (NA) Plan-Apochromat objective (Carl Zeiss Microimaging) with glycerol as immersion medium. Fluorescence excitation was provided by either a Chameleon XR Ti:sapphire laser (Coherent) for the LSM 510 NLO or an Insight Ds+ (Spectra Physics) for the LSM 780 NLO tuned to 850 nm for dye excitation and the generation of collagen second harmonic signal, or 940 nm for excitation of both DsRed and green fluorescent protein (GFP). Non-descanned detectors collected the emitted light. For four-dimensional (4D) datasets, 3D stacks were captured every 30 s, unless otherwise specified. All imaged mice were on the *Tyr*$^{c\text{-}2J/c\text{-}2J}$ (B6.Albino) background to avoid laser-induced cell death of light-sensitive skin melanophages. Raw imaging data were processed with Imaris (Bitplane) using a Gaussian filter for noise reduction. All movies are displayed as 2D maximum-intensity projections of 10-to 30-μm-thick *z*-stacks.

### Mouse infection and 2P-IVM of neutrophil swarms in lymph nodes

GFP-expressing *P. aeruginosa PAO1* (PA) (61) or *Salmonella typhimurium SL1344* (62), both provided through W. Kastenmüller (University Würzburg, Germany), were grown for 1 to 4 hours in LB medium to reach an $OD_{600nm}$ of 0.6 to 0.7 in the exponential growing culture, before $10^7$ colony-forming units (CFU) of bacteria were diluted in PBS and injected in the mouse foot-pad (20 to 30 μl) as described (29). To image endogenous wild-type and GRK2-depleted neutrophils side-by-side in bacteria-infected lymph nodes,

we generated bone marrow chimeric mice. C57BL/6 mice were irradiated with 9 Gray from a $^{137}$Cs source and reconstituted with bone marrow from *Ly6g*$^{cre/+}$ *Rosa26*$^{LSL:Tomato}$ mice (wild-type, tdTomato-expressing neutrophils) and *Mrp8-Cre*$^{+/-}$ *Grk2*$^{fl/fl}$ *Lyz2*$^{gfp/+}$ mice (GRK2-depleted, neutrophils with highest expression of GFP) at a 1:1 ratio. Mice were allowed to reconstitute for at least 8 weeks before imaging analysis. 2P-IVM of transient neutrophil swarms in the SCS of bacteria-infected lymph nodes was performed as described (9). Two to three hours after injection, mice were anesthetized with isoflurane (Baxter; 2% for induction, 1 to 1.5% for maintenance, vaporized in an 80:20 mixture of $O_2$ and air), before draining popliteal lymph nodes were exposed and intravital microscopy performed. The imaging system was composed of a tuneable Chameleon laser (Coherent) tuned to 930 nm, a wavelength-fixed fiber laser (1055 nm) (Onefive GmbH) and a Zeiss 780 upright microscope equipped with a 20× water immersion lens (NA 1.0, Zeiss) and ZEN acquisition control software. The microscope was enclosed in an environmental chamber in which anesthetized mice were warmed by heated air and the surgically exposed lymph node was kept at 36° to 37°C with warmed PBS. For 2P-IVM of the SCS, a *z*-stack of 40 to 50 μm, 3-μm step size was used and images were acquired every 40 s. Raw imaging data processing and movie display was similar as for 2P-IVM ear skin datasets. To analyze the containment of bacterial growth in lymph nodes, $10^7$ CFU of *P. aeruginosa* PAO1-GFP (PA-GFP) were injected in mouse footpads of *Mrp8-Cre*$^{+/-}$ *Grk2*$^{fl/fl}$ mice and sex- and age-matched littermate control mice. Control mice were either Cre-negative *Grk2*$^{fl/fl}$ or *Mrp8-Cre*$^{+/-}$ *Grk2*$^{+/+}$ mice, depending on the breeder cage setup. For the quantification of bacterial load, popliteal lymph nodes were harvested 8 hours after infection and lymph node homogenates were plated on blood-agar plates overnight, before bacterial colonies were counted. Neutrophil recruitment into infected popliteal lymph nodes was measured by flow cytometry in single-cell suspension of lymph node homogenates 8 hours after infection, identifying neutrophils as a live Ly6G$^+$CD11b$^+$ leukocyte population. Exclusion criteria for individual values included the absence of bacterial growth or neutrophil recruitment due to improper bacterial injection.

### In vitro coculture model

To mimic a bacteria-infected SCS in vitro, macrophages were cocultured with GFP-expressing *P. aeruginosa* PAO1 (PA-GFP) (61) in the presence and absence of neutrophils. Bone marrow–derived mouse macrophages (BMDM) were generated from bone marrow precursors by standard M-CSF culture. Bone marrow cells were suspended in macrophage culture medium and grown over 6 days on Petri dishes in macrophage culture medium [10% FBS, penicillin (100 U/ml), and streptomycin (10 μg/ml) in RPMI GlutaMax] supplemented with murine M-CSF (20 ng/ml; PeproTech). PA-GFP were grown in LB medium for 16 hours at 37°C until $OD_{600nm}$ 0.6 to 0.7. When macrophages were infected with bacteria in the absence of neutrophils, experiments were performed in eight-well Lab-Tek imaging chamber slides that were coated with fibronectin from human plasma (10 μg/ml; Sigma-Aldrich, cat. no. F2006) overnight at 4°C. For macrophage infection experiments, CellTracker Blue–labeled macrophages were taken up in phenol-red free RPMI supplemented with 10% FCS and 2 mM L-glutamine, then seeded at 80 × $10^3$ cells per well and allowed to adhere for 3 hours at 37°C. PA-GFP in RPMI with 2 mM L-glutamine was then added to BMDM at a ratio of 10 bacteria per one macrophage in the presence of propidium

iodide (5 μg/ml; BioLegend). For coculture experiments of macrophages with bacteria and neutrophils, experiments were performed in μ-Slide VI 0.4 channels (Ibidi, cat. no. 80606) that were coated with fibronectin (10 μg/ml) overnight at 4°C. Dye-labeled or unlabeled BMDM were seeded at ~$15 \times 10^3$ cells per channel and allowed to adhere for 3 hours at 37°C. Bacteria and neutrophils were added through separate ports of the slide: 60 μl of the neutrophil suspension at $13 \times 10^6$ cells/ml in RPMI with 2 mM L-glutamine and 20% freshly collected mouse serum were added to the first port and 60 μl of PA-GFP ($3 \times 10^7$ CFU/ml) suspension were added to the second port, before live-cell imaging was initiated. When control and GRK2-depleted neutrophils were analyzed side by side in the well, they were differentially labeled with 5-TAMRA SE, and CellTracker Deep Red, whereas macrophages remained unlabeled. To follow PA-GFP that was phagocytosed by neutrophils, PA-GFP was labeled with pHrodo succinimidyl ester (2.5 μg/ml; Thermo Fisher Scientific, cat no. P36600) in 500 μl of freshly prepared 100 mM sodium bicarbonate buffer (pH 8.5) for 30 min at room temperature. Afterward, bacteria were washed three times with 1× PBS to remove any remaining dye. When visualization of dying cells was required, propidium iodide (5 μg/ml) or DAPI (1 μg/ml; Sigma-Aldrich) were added to the medium. Macrophage infection with bacteria and neutrophil swarming and clustering were followed by confocal fluorescence laser-scanning microscopy using a confocal LSM 780 microscope (Zeiss) equipped with a stage top incubator to generate an ambient atmosphere of 37°C and 5% $CO_2$ and objectives. Time-lapse videos were recorded using Plan Apochromat 20× (0.8 NA) and C Apochromat 40× (1.2 NA) objectives with image acquisitions every 5 min over 8 hours, 15-μm *z*-stacks and 2×2 tiled images. Tiled images were stitched during postprocessing with ZEN Blue software. Images were acquired using up to four–laser line excitation (UV405 for CellTracker Blue; Argon488 for PA-GFP, DPSS561 for 5-TAMRA SE, or SYTOX Orange or propidium iodide; HeNe633 for CellTracker Deep Red). The internal photomultiplier tubes and GaAsP detector of the confocal system were used for collecting the emitted fluorescence light.

### Data analysis of neutrophil in vitro migration

Neutrophil displacement in the under-agarose assay from a starting well toward a chemotactic source well was measured with Imaris software (Bitplane). After 4 hours of chemotaxis, images of neutrophils that migrated out of the cell well were acquired as endpoint measurements and cell center points identified with Imaris spot function. The displacement was measured as the distance from the border of the starting cell well to the migration endpoints of all neutrophils that migrated underneath the agarose toward the attractant well. The mean of all individual displacement values was calculated for each genotype. For displacement ratios, the ratio of wild-type and $Grk^{-/-}$ neutrophils, which migrated side by side from one well, was calculated and the mean ratios of all four technical replicates were determined and plotted as an independent experiment. In some cases (Fig. 1G and fig. S2A), the mean displacement of all four technical replicates in one dish was determined for wild-type or $Grk^{-/-}$ and plotted side by side as an independent experiment. In rare cases, technical replicates were excluded from analysis when neutrophils did not respond to the attractant and only very few cells migrated out of the well. Live-cell imaging data of neutrophil chemotaxis in under-agarose assays was visualized (neutrophil trajectories) and analyzed for migration parameters (track length,

straightness, *y*-straightness, velocity vector Y, instantaneous speed, and cell roundness) by Imaris manual object cell tracking and statistics functions. For some experiments, the resultant spatial coordinates over time were further processed to retrieve displacement-time plots by computation using R software (version 4.0.2), R studio (version 1.3.959), and ggplot2 (version 3.3.2). To quantify neutrophil sequential navigation in under-agarose gels with multiple attractant sources (Fig. 3A and fig. S6, B and C), a semi-automated tracking approach was applied. The autoregressive tracking mode of the Imaris spot function was used for automated cell tracking, followed by manual inspection of track validity. Cell displacement lengths in *y*- (toward first gradient/up) and *x*- (toward second gradient/right) directions were derived from Imaris statistic function. To analyze migration arrest in neutrophil clusters (Fig. 4E), individual cells ($N = 7$ to 22 cells per cluster) were manually tracked for 3 to 4 hours in cell clusters and instantaneous speed values retrieved from Imaris. Integration into a cluster for longer than 8 min was a criterion for tracking the total movement of a neutrophil. For one cluster, the instantaneous velocities of all cells were determined. An instantaneous speed of <2 μm/min was defined as cell arrest phase, as described (63). The arrest coefficient was calculated as the percentage of arrest phases from all instantaneous speed values of all cells tracked at one cluster. To analyze the competitive accumulation of neutrophils and eosinophils in clusters during in vitro swarming experiments (Fig. 2, B and I, and fig. S4B), total fluorescent signals of control and *Grk2*$^{-/-}$ cells in the whole cell cluster area were quantified with ImageJ/Fiji software (NIH). Accumulation indices were then calculated as the ratio of *Grk2*$^{-/-}$ signal to wild-type signal on HKSA spots after 2 hours and compared to experiments in which two differentially labeled wild-type populations formed competitive clusters. Accumulation indices were displayed in graphs with $\log_2$-scaled *y* axis.

### Data analysis of neutrophil in vivo migration

Data from neutrophil migration dynamics recorded with 2P-IVM were visualized (neutrophil trajectories, velocity vector Y, instantaneous speed) and analyzed for migration parameters (track length, straightness, speed) by Imaris manual object cell tracking and statistics functions. To quantify neutrophil clustering in vivo, accumulation indices were calculated. In 2P-IVM laser damage experiments in the skin, the accumulation index as measure of cell entry into the collagen-free zone was defined as the ratio of fluorescent signal from *Grk*$^{-/-}$ cells in the collagen-free zone versus total signal at the wound site divided by the ratio of fluorescent signal from control cells in the collagen-free zone versus total signal at the wound site, as defined in (9). Accumulation indices were calculated when neutrophil cluster size was at its maximum and clusters stabilized. In the skin, this commonly occurred 30 to 75 min after laser-induced tissue injury, depending on the specific dynamics of an individual neutrophil cluster. Because of the lack of clear collagen signal in lymph node areas, the accumulation index for lymph node infection experiments was defined as the ratio of fluorescent signal from *Grk2*$^{-/-}$ neutrophils in the inner zone (= 50% diameter of total cell cluster zone) versus total signal at the whole neutrophil cluster divided by the ratio of fluorescent signal from control cells in the inner zone versus total signal at the neutrophil cluster. Fluorescent signals were quantified with ImageJ/Fiji software. Accumulation indices were displayed in graphs with $\log_2$-scaled *y* axis. For the display of

static images and videos, raw imaging data were processed with Imaris using a Gaussian filter for noise reduction.

### Analysis of bacterial growth and phagocytosis in the coculture assay

Bacterial growth in cocultures with neutrophils and macrophages was analyzed by quantifying fluorescent signals of GFP-expressing *P. aeruginosa* (PA-GFP) bacteria with Imaris software. By generating surfaces from fluorescent bacteria, “total” bacteria were quantified as total area of PA-GFP surfaces. To determine the fraction of bacteria “confined” to neutrophil clusters (illustrated in white in Fig. 4B), the surfaces of fluorescent bacteria and CellTracker-labeled neutrophils were co-localized. Exclusion of colocalization surfaces less than 250 $\mu m^2$ was performed to exclude the very small fraction (4 to 8%) of bacterialaden individual neutrophils outside of clusters. “Free” bacteria signal outside of neutrophils (illustrated in green in Fig. 4B) was calculated by subtracting the surface areas of “confined” bacteria to neutrophils from “total” bacteria. To quantify the fraction of pHrodo-tagged, phagocytosed PA-GFP, the fluorescence of the pHrodo signal was measured per neutrophil cell cluster using Imaris software. To quantify bacteria containment within neutrophil clusters, we used ImageJ/Fiji software to draw two outlines around a bacteria cluster surrounded neutrophils: one defined the perimeter of the complete bacteria cluster, the other defined the perimeter part in direct contact with clustering neutrophils. Bacteria containment was calculated as the percentage of the perimeter in direct contact with neutrophils from the complete bacteria cluster perimeter.

### Determination of knockout efficiencies

To determine knockout efficiencies in neutrophils isolated from conditional knockout mice, quantitative real-time PCR (qRT-PCR) and immunoblot analysis were performed. For qRT-PCR, total RNA of bone marrow neutrophils was extracted using TRI Reagent solution (Sigma-Aldrich). Briefly, the aqueous RNA-containing phase was extracted with chloroform. The RNA was precipitated in 2-propanol overnight at –20°C. The RNA pellet was washed twice in 80% ethanol. DNase treatment was performed using TURBO DNA-free Kit (Ambion). Reverse transcription was performed using SuperScript II reverse transcriptase and random hexamer primers following the manufacturer’s instructions (Invitrogen). Quantitative PCR was performed using a SYBR Green master mix cocktail (Thermo Fisher Scientific). cDNA amplification and quantification were performed in a StepOnePlus real-time PCR machine (Applied Biosystems). Gene expression levels of *Grk2*, *Grk3*, *Grk5*, and *Grk6* were normalized against 18*S* rRNA, *B2m*, and *Actb* as reference genes. See table S2 for details on primers. For immunoblot analysis, neutrophils were first lysed in freshly prepared RIPA buffer (50 mM Tris-HCl, 150 mM NaCl, 1.0% (v:v) IGEPAL CA-630, 1% (v:v) Triton X-100, 5 mM EGTA, 5 mM EDTA, and 1× cOmplete protease inhibitor cocktail). Proteins were separated by 4 to 12% SDS-PAGE gels (BioRad) and then transferred onto PVDF membranes (Millipore) and nonspecific binding was blocked with 5% BSA (Sigma-Aldrich) in Tris-buffered saline containing 0.1% Tween 20, followed by overnight incubation with primary antibodies against GRK2 (SCBT) and actin as control (Sigma-Aldrich). Membranes were subsequently washed and incubated with the appropriate secondary antibodies (Dako), and immunoreactivity was detected upon incubation with Clarity Western ECL substrate (BioRad) using ChemiDoc Imaging System (BioRad). The

same protocol was used for the determination of GRK2 knockout efficiency in eosinophils (see below). For details on the use of antibodies, see table S4.

### Flow cytometric analysis of neutrophil subpopulations

Neutrophil subsets in bone marrow and blood were analyzed by flow cytometry as described (64). Nonspecific binding was blocked with anti-mouse CD16/CD32. Fixable Viability Dye eFluor506 (Thermo Fisher Scientific) was used to stain dead cells. Antibodies and reagents used for flow cytometry are summarized in table S4. Flow cytometric analysis was performed using an LSRFortessa (BD Biosciences) flow cytometer, FACSDiva software (BD Bio-sciences), and FlowJo software (FlowJo LLC). For the analysis of neutrophils in the bone marrow, gating started with Lineage (B220, CD3e, CD90.2, NK1.1)$^-$ cells. Blood neutrophils were gated on (Lineage$^-$CD115$^-$SiglecF$^-$ Gr1$^+$CD11b$^+$) cells.

### Receptor internalization

Surface receptor expression after ligand stimulation was measured by flow cytometry. Neutrophils were stimulated with 200 nM LTB4 or 50 nM CXCL2 for the indicated time points at 37°C. Then, cells were incubated on ice to halt receptor internalization. Flow cytometric staining for LTB4R1 and CXCR2 (see table S4 for details on antibodies) was performed as described with all steps at 4°C.

### Neutrophil GPCR desensitization: MAPK signaling and GPCR-induced chemokinesis

To measure activation of MAPK signaling cascades downstream of GPCR activation, neutrophils were stimulated with GPCR ligands (LTB4, CXCL2, C5a) for the indicated time points followed by fixation in 1.6% paraformaldehyde (Thermo Fisher Scientific) and permeabilization in 100% methanol at –20°C overnight. Cells were stimulated with individual attractants for 2 min. For triple stimulations with increasing concentrations of LTB4 (50 nM, 100 nM, and 200 nM), CXCL2 (50 nM, 100 nM, and 200 nM), or C5a (5 nM, 10 nM, and 20 nM), cells were treated for 4 min (first stimulation), 4 min (second stimulation), and 2 min (third stimulation). For the intracellular antibody stainings, nonspecific binding was blocked with anti-mouse CD16/CD32 and 5% rabbit serum (Thermo Fisher Scientific) in 1× PBS. Neutrophils were then stained with directly fluorescent anti-mouse antibodies to p-p38 MAPK and p-p44/42 (see table S4). Flow cytometric analysis was performed using an LSRFortessa (BD Biosciences) flow cytometer, FACSDiva software (BD Biosciences) and FlowJo software (FlowJo, LLC).

To measure the effect of GPCR desensitization on chemokinesis, wild-type and *Grk2*$^{-/-}$ neutrophils were pretreated with attractant concentrations that desensitize GPCR-induced calcium responses in wild-type cells: LTB4 (50 nM, 100 nM, and 200 nM), CXCL2 (50 nM and 100 nM), and CXCL2 (10 nM, 20 nM, and 40 nM) according to the time scheme described above. For these experiments, wild-type and *Grk2*$^{-/-}$ neutrophils were isolated from *Mrp8-Cre Grk2*$^{+/+}$ *R26*$^{LSL:Tom}$ (wild-type, red) and *Mrp8-Cre Grk2*$^{fl/fl}$ *Lyz2*$^{Gfp/+}$ (*Grk2*$^{-/-}$, green) mice, or alternatively from *Mrp8-Cre Grk2*$^{fl/fl}$ *R26*$^{LSL:Tom}$ (KO, red) and *Mrp8-Cre Grk2*$^{+/+}$ *Lyz2*$^{Gfp/+}$ (wild-type, green) mice. Pretreated, differentially color-labeled wild-type and *Grk2*$^{-/-}$ neutrophils were loaded into the same µ-Slide VI 0.4 channel, which was coated with human recombinant ICAM-1 (Peprotech, 1 µg/ml), and were immediately

imaged side by side with confocal spinning-disk microscopy. We used the Cell Observer SD system (Zeiss) comprising a CSU-X1 confocal scanner unit (Yokogawa) mounted on an AxioObserver Z1 inverted microscope stand, and equipped with a Prime BSI back-illuminated CMOS camera (Teledyne Photometrics). A Plan-Apochromat 10× 0.45 objective (Zeiss) and excitation with 488-nm and 561-nm solid-state lasers were used in order to observe neutrophils with a frame rate of 30 s over 45 min. Randomly chosen cells were tracked with Imaris spot function and statistics function to retrieve cell positions for the display of cell tracks with R ggplot2 function.

### Assays for neutrophil effector functions

Neutrophil myeloperoxidase (MPO) release was measured with ELISA according to the manufacturer's instructions (R&D Systems; cat no. DY3667). Neutrophil elastase (NE) activity was determined using the EnzCheck elastase assay kit following the manufacturer's instructions (Thermo Fisher Scientific; cat no. E12056). MPO and NE release were determined in supernatants of neutrophils stimulated with 100 nM LTB4 and 100 nM CXCL2 for 2 hours. Reactive oxygen species (ROS) production was quantified by determining the superoxide dismutase (SOD) inhibitable reduction of (ferri-) cytochrome c as described (65). Briefly, neutrophils were stimulated with 100 nM LTB4 and 100 nM CXCL2, heat-killed *P. aeruginosa* bioparticles (HKPA, at a ratio of 100 particles to one cell) (Invivogen), zymosan (10 μg/ml; Thermo Fisher Scientific), or 10 nM phorbol-12-myristate-13-acetate (PMA, Sigma-Aldrich) in the presence of 100 μM cytochrome c from equine heart (Thermo Fisher Scientific). As control for nonspecific cytochrome c reduction, simultaneous assays were performed in the presence of 100 U/ml of SOD, and the SOD-inhibitable signal was determined. The release of ROS was measured every minute for1 hour by light absorbance at 550 nm (wavelength correction at 490 nm) using a Synergy4 plate reader (Bio-Tek) heated to 37°C. As standard measure for neutrophil phagocytosis, neutrophils were co-incubated for 1 hour with opsonized *S. aureus* pHrodo bioparticles (Thermo Fisher Scientific; cat no. A10010) at a ratio of 100:1 in the absence orpresence of LTB4 and CXCL2 (100 nM each), before particle uptake was analyzed by flow cytometry. To measure internalization of living *P. aeruginosa*, tdTomato-expressing neutrophils were co-incubated with PAO1-GFP at MOI = 20. Cells and bacteria were co-incubated in a 1.5-ml reaction tube in a total volume of 100 μl of phenol red–free RPMI supplemented with 20% mouse serum (VWR, cat no. S2160–050) and 2 mM L-glutamine in the absence or presence of LTB4/CXCL2 (100 nM each), and placed in a shaking heat block at 450 rpm, 37°C for 60 min. tdTomato-expressing wild-type or $Grk2^{-/-}$ neutrophils were isolated from *Mrp8-Cre* $Grk2^{+/+}$ $R26^{LSL:Tom}$ or *Mrp8-Cre* $Grk2^{fl/fl}$ $R26^{LSL:Tom}$ mice, respectively. After the 1-hour co-incubation, 60 μl of the cell/bacteria suspension was transferred into μ-Slide VI 0.4 channels (Ibidi). Fluorescent neutrophils and bacteria were imaged with a confocal LSM 780 microscope (Zeiss) equipped with a stage-top incubator to generate an ambient atmosphere of 37°C and 5% $CO_2$. Images were recorded using Plan Apochromat 20× (0.8 NA) at 1024×1024 resolution and 7×7 tiles. Imaris surface and spot functions were used to determine GFP-positive signals located inside surfaces of red neutrophils (fig. S8B). Per experimental condition, ~200 to 1000 neutrophils were analyzed and the percentage of neutrophils with internalized bacteria was calculated. To identify and quantify NET-like structures in the coculture assay with PAO1-GFP and macrophages, 10 nM

SYTOX Orange nucleic acid stain (Thermo Fisher Scientific) was added to the medium. Confocal microscopy of SYTOX Orange fluorescent signal was recorded, before surfaces of the SYTOX Orange fluorescent signal were generated with Imaris software. Total surface areas were quantified after exclusion of surfaces less than 250 $\mu m^2$ that were considered non–NET-like structures.

### Design and statistical analysis

Sample size was determined prior to experiment for all experiments used for hypothesis testing (i.e., data that include statistical inference). Sample size for animal experimentation was determined according to animal welfare guidelines. Reproducibility of the experimental findings was verified using biological replicates. Experimental groups were defined by the genotype. Blinding was not relevant to our study because all experimental groups (genotype groups) were treated the same. Unpaired two-tailed *t* tests, paired *t* tests for ratios, and analysis of variance (ANOVA) were performed after data were confirmed to fulfill the criteria of normal distribution and equal variance, otherwise two-tailed Kruskal-Wallis tests or Mann-Whitney *U* tests were applied. If overall ANOVA or Kruskal-Wallis tests were significant, we performed a post hoc test with pairwise comparisons (ANOVA: Tukey, Kruskal-Wallis: Dunn). Analyses were performed with GraphPad Prism-software (8.2.1 and 9.0.2). For further statistical details, see table S3.

## Supplementary Material

Refer to Web version on PubMed Central for supplementary material.

## ACKNOWLEDGMENTS

We thank R. Wedlich-Söldner for kindly providing mice for this study; R. Thünauer and W. Römer for initial help with bacterial work; D. Legler for helpful advice; members of the MPI Imaging Facility for assistance with imaging; and K. Ganter and L. Kaltenbach for assistance with experiments and analysis.

**Funding:**

Supported by the Max Planck Society (T.L., W.K.); the Deutsche Forschungsgemeinschaft (LA3465/1-1, SFB/CRC167-A06, and CRC850-A03, T.L.; Germany's Excellence Strategy EXC-294 and EXC-2189:390939984, CRC850-A06, and CRC1381-B09, R.B.); ERC Starting Grant 715890 (T.L.); ERC Consolidator Grant 819329 (W.K.); the Ministry of Culture and Science of North Rhine–Westphalia, the Governing Mayor of Berlin including Science and Research, and the Federal Ministry of Education and Research (BMBF) (M.G.); Chan Zuckerberg Initiative grant 2020-217723 (E.R.,T.L.); the Intramural Research Program of the National Institute of Allergy and Infectious Diseases (NIAID) (R.N.G.); and NIAID grant AI113937 (D.I.).

## REFERENCES AND NOTES

1. Breed MD, Guzmán-Novoa E, Hunt GJ, Defensive behavior of honey bees: Organization, genetics, and comparisons with other bees. Annu. Rev. Entomol 49, 271–298 (2004). doi: 10.1146/annurev.ento.49.061802.123155 [PubMed: 14651465]
2. Guo X et al. , 4-Vinylanisole is an aggregation pheromone in locusts. Nature 584, 584–588 (2020). doi: 10.1038/s41586-020-2610-4 [PubMed: 32788724]
3. Mahadeo DC, Parent CA, Signal relay during the life cycle of Dictyostelium. Curr. Top. Dev. Biol 73, 115–140 (2006). doi: 10.1016/S0070-2153(05)73004-0 [PubMed: 16782457]
4. Ley K et al. , Neutrophils: New insights and open questions. Sci. Immunol 3, eaat4579 (2018). doi: 10.1126/sciimmunol.aat4579 [PubMed: 30530726]

5. Neupane ASW et al. , Patrolling Alveolar Macrophages Conceal Bacteria from the Immune System to Maintain Homeostasis. Cell 183, 110–125.e11 (2020). doi: 10.1016/j.cell.2020.08.020 [PubMed: 32888431]
6. Uderhardt S, Martins AJ, Tsang JS, Lämmermann T, Germain N, Resident Macrophages Cloak Tissue Microlesions to Prevent Neutrophil-Driven Inflammatory Damage. Cell 177, 541–555.e17 (2019). doi: 10.1016/j.cell.2019.02.028 [PubMed: 30955887]
7. Kienle K, Lämmermann T, Neutrophil swarming: An essential process of the neutrophil tissue response. Immunol. Rev 273, 76–93 (2016). doi: 10.1111/imr.12458 [PubMed: 27558329]
8. Weninger W, Biro M, Jain R, Leukocyte migration in the interstitial space of non-lymphoid organs. Nat. Rev. Immunol 14, 232–246 (2014). doi: 10.1038/nri3641 [PubMed: 24603165]
9. Lämmermann T et al. , Neutrophil swarms require LTB4 and integrins at sites of cell death in vivo. Nature 498, 371–375 (2013). doi: 10.1038/nature12175 [PubMed: 23708969]
10. Coombs C et al. , Chemokine receptor trafficking coordinates neutrophil clustering and dispersal at wounds in zebrafish. Nat. Commun 10, 5166 (2019). doi: 10.1038/s41467-019-13107-3 [PubMed: 31727891]
11. Poplimont H et al. , Neutrophil Swarming in Damaged Tissue Is Orchestrated by Connexins and Cooperative Calcium Alarm Signals. Curr. Biol 30, 2761–2776.e7 (2020). doi: 10.1016/j.cub.2020.05.030 [PubMed: 32502410]
12. Reátegui E et al. , Microscale arrays for the profiling of start and stop signals coordinating human-neutrophil swarming. Nat. Biomed. Eng 1, 0094 (2017). doi: 10.1038/s41551-017-0094 [PubMed: 29057147]
13. Freedman NJ, Lefkowitz RJ, Desensitization of G protein-coupled receptors. Recent Prog. Horm. Res 51, 319–351 (1996). [PubMed: 8701085]
14. Lämmermann T, Kastenmüller W, Concepts of GPCR-controlled navigation in the immune system. Immunol. Rev 289, 205–231 (2019). doi: 10.1111/imr.12752 [PubMed: 30977203]
15. Rose JJ, Foley JF, Murphy PM, Venkatesan S, On the mechanism and significance of ligand-induced internalization of human neutrophil chemokine receptors CXCR1 and CXCR2. J. Biol. Chem 279, 24372–24386 (2004). doi: 10.1074/jbc.M401364200 [PubMed: 15028716]
16. Tomhave ED et al. , Cross-desensitization of receptors for peptide chemoattractants. Characterization of a new form of leukocyte regulation. J. Immunol 153, 3267–3275 (1994). [PubMed: 8089498]
17. Fan J, Malik AB, Toll-like receptor-4 (TLR4) signaling augments chemokine-induced neutrophil migration by modulating cell surface expression of chemokine receptors. Nat. Med 9, 315–321 (2003). doi: 10.1038/nm832 [PubMed: 12592402]
18. Kavelaars A et al. , Increased acute inflammation, leukotriene B4-induced chemotaxis, and signaling in mice deficient for G protein-coupled receptor kinase 6. J. Immunol 171, 6128–6134 (2003). doi: 10.4049/jimmunol.171.11.6128 [PubMed: 14634128]
19. Raghuwanshi SK et al. , The chemokine receptors CXCR1 and CXCR2 couple to distinct G protein-coupled receptor kinases to mediate and regulate leukocyte functions. J. Immunol 189, 2824–2832 (2012). doi: 10.4049/jimmunol.1201114 [PubMed: 22869904]
20. Tarrant TK et al. , G protein-coupled receptor kinase-3-deficient mice exhibit WHIM syndrome features and attenuated inflammatory responses. J. Leukoc. Biol 94, 1243–1251 (2013). doi: 10.1189/jlb.0213097 [PubMed: 23935208]
21. Vroon A et al. , GRK6 deficiency is associated with enhanced CXCR4-mediated neutrophil chemotaxis in vitro and impaired responsiveness to G-CSF in vivo. J. Leukoc. Biol 75, 698–704 (2004). doi: 10.1189/jlb.0703320 [PubMed: 14704365]
22. Arnon TI et al. , GRK2-dependent S1PR1 desensitization is required for lymphocytes to overcome their attraction to blood. Science 333, 1898–1903 (2011). doi: 10.1126/science.1208248 [PubMed: 21960637]
23. Evron T, Daigle TL, Caron MG, GRK2: Multiple roles beyond G protein-coupled receptor desensitization. Trends Pharmacol. Sci 33, 154–164 (2012). doi: 10.1016/j.tips.2011.12.003 [PubMed: 22277298]
24. Aratake Y et al. , Helix 8 of leukotriene B4 receptor 1 inhibits ligand-induced internalization. FASEB J 26, 4068–4078 (2012). doi: 10.1096/fj.12-212050 [PubMed: 22707565]

25. Subramanian BC, Moissoglu K, Parent CA, The $LTB_4$-BLT1 axis regulates the polarized trafficking of chemoattractant GPCRs during neutrophil chemotaxis. J. Cell Sci 131, jcs.217422 (2018). doi: 10.1242/jcs.217422
26. Mishra HK, Long C, Bahaie NS, Walcheck B, Regulation of CXCR2 expression and function by a disintegrin and metalloprotease-17 (ADAM17). J. Leukoc. Biol 97, 447–454 (2015). doi: 10.1189/jlb.3HI0714-340R [PubMed: 25412626]
27. Patnode ML, Bando JK, Krummel MF, Locksley RM, Rosen D, Leukotriene B4 amplifies eosinophil accumulation in response to nematodes. J. Exp. Med 211, 1281–1288 (2014). doi: 10.1084/jem.20132336 [PubMed: 24889202]
28. Foxman EF, Campbell JJ, Butcher EC, Multistep navigation and the combinatorial control of leukocyte chemotaxis. J. Cell Biol 139, 1349–1360 (1997). doi: 10.1083/jcb.139.5.1349. [PubMed: 9382879]
29. Kastenmüller P Torabi-Parizi, N. Subramanian, Lämmermann, R. N. Germain, A spatially-organized multicellular innate immune response in lymph nodes limits systemic pathogen spread. Cell 150, 1235–1248 (2012). doi: 10.1016/j.cell.2012.07.021 [PubMed: 22980983]
30. Dacheux D, Goure J, Chabert J, Usson Y, Attree I, Poreforming activity of type III system-secreted proteins leads to oncosis of Pseudomonas aeruginosa-infected macrophages. Mol. Microbiol 40, 76–85 (2001). doi: 10.1046/j.1365-2958.2001.02368.x [PubMed: 11298277]
31. Thanabalasuriar A et al. , Neutrophil Extracellular Traps Confine Pseudomonas aeruginosa Ocular Biofilms and Restrict Brain Invasion. Cell Host Microbe 25, 526–536.e4 (2019). doi: 10.1016/j.chom.2019.02.007 [PubMed: 30930127]
32. Heit B, Tavener S, Raharjo E, Kubes P, An intracellular signaling hierarchy determines direction of migration in opposing chemotactic gradients. J. Cell Biol 159, 91–102 (2002). doi: 10.1083/jcb.200202114 [PubMed: 12370241]
33. Hopke A et al. , Neutrophil swarming delays the growth of clusters of pathogenic fungi. Nat. Commun 11, 2031 (2020). doi: 10.1038/s41467-020-15834-4 [PubMed: 32341348]
34. Waite JC et al. , Dynamic imaging of the effector immune response to listeria infection in vivo. PLOS Pathog 7, e1001326 (2011). doi: 10.1371/journal.ppat.1001326 [PubMed: 21455492]
35. Liu X et al. , Bidirectional regulation of neutrophil migration by mitogen-activated protein kinases. Nat. Immunol 13, 457–464 (2012). doi: 10.1038/ni.2258 [PubMed: 22447027]
36. Wang G et al. , Oxidant Sensing by TRPM2 Inhibits Neutrophil Migration and Mitigates Inflammation. Dev. Cell 38, 453–462 (2016). doi: 10.1016/j.devcel.2016.07.014 [PubMed: 27569419]
37. Chabaud M et al. , Cell migration and antigen capture are antagonistic processes coupled by myosin II in dendritic cells. Nat. Commun 6, 7526 (2015). doi: 10.1038/ncomms8526 [PubMed: 26109323]
38. Evans IR, Ghai PA, Urbančič V, Tan KL, Wood W, SCAR/WAVE-mediated processing of engulfed apoptotic corpses is essential for effective macrophage migration in Drosophila. Cell Death Differ 20, 709–720 (2013). doi: 10.1038/cdd.2012.166 [PubMed: 23328632]
39. Faure-André G et al. , Regulation of dendritic cell migration by CD74, the MHC class II-associated invariant chain. Science 322, 1705–1710 (2008). doi: 10.1126/science.1159894 [PubMed: 19074353]
40. Lavi I, Piel M, Lennon-Dumenil AM, Voituriez R, Gov NS, Deterministic patterns in cell motility. Nat. Phys 12, 1146–1152 (2016). doi: 10.1038/nphys3836
41. Pan M, Xu X, Chen Y, Jin T, Identification of a Chemoattractant G-Protein-Coupled Receptor for Folic Acid that Controls Both Chemotaxis and Phagocytosis. Dev. Cell 36, 428–439 (2016). doi: 10.1016/j.devcel.2016.01.012 [PubMed: 26906738]
42. Veltman DM, Lemieux MG, Knecht DA, Insall RH, $PIP_3$-dependent macropinocytosis is incompatible with chemotaxis. J. Cell Biol 204, 497–505 (2014). doi: 10.1083/jcb.201309081 [PubMed: 24535823]
43. Wen X et al. , G-protein-coupled formyl peptide receptors play a dual role in neutrophil chemotaxis and bacterial phagocytosis. Mol. Biol. Cell 30, 346–356 (2019). doi: 10.1091/mbc.E18-06-0358 [PubMed: 30540534]

44. Dong YH, Zhang LH, Quorum sensing and quorum-quenching enzymes. J. Microbiol 43, 101–109 (2005). [PubMed: 15765063]
45. Tweedy L et al. , Seeing around corners: Cells solve mazes and respond at a distance using attractant breakdown. Science 369, eaay9792 (2020). doi: 10.1126/science.aay9792 [PubMed: 32855311]
46. Passegué E, Wagner EF, Weissman IL, JunB deficiency leads to a myeloproliferative disorder arising from hematopoietic stem cells. Cell 119, 431–443 (2004). doi: 10.1016/j.cell.2004.10.010 [PubMed: 15507213]
47. Matkovich SJ et al. , Cardiac-specific ablation of G-protein receptor kinase 2 redefines its roles in heart development and beta-adrenergic signaling. Circ. Res 99, 996–1003 (2006). doi: 10.1161/01.RES.0000247932.71270.2c [PubMed: 17008600]
48. Peppel K et al. , G protein-coupled receptor kinase 3 (GRK3) gene disruption leads to loss of odorant receptor desensitization. J. Biol. Chem 272, 25425–25428 (1997). doi: 10.1074/jbc.272.41.25425 [PubMed: 9325250]
49. Gainetdinov RR et al. , Muscarinic supersensitivity and impaired receptor desensitization in G protein-coupled receptor kinase 5-deficient mice. Neuron 24, 1029–1036 (1999). doi: 10.1016/S0896-6273(00)81048-X [PubMed: 10624964]
50. Gainetdinov RR et al. , Dopaminergic supersensitivity in G protein-coupled receptor kinase 6-deficient mice. Neuron 38, 291–303 (2003). doi: 10.1016/S0896-6273(03)00192-2 [PubMed: 12718862]
51. Faust N, Varas F, Kelly LM, Heck S, Graf T, Insertion of enhanced green fluorescent protein into the lysozyme gene creates mice with green fluorescent granulocytes and macrophages. Blood 96, 719–726 (2000). doi: 10.1182/blood.V96.2.719 [PubMed: 10887140]
52. Hasenberg A et al. , Catchup: A mouse model for imaging-based tracking and modulation of neutrophil granulocytes. Nat. Methods 12, 445–452 (2015). doi: 10.1038/nmeth.3322 [PubMed: 25775045]
53. de Boer J et al. , Transgenic mice with hematopoietic and lymphoid specific expression of Cre. Eur. J. Immunol 33, 314–325 (2003). doi: 10.1002/immu.200310005 [PubMed: 12548562]
54. Vintersten K et al. , Mouse in red: Red fluorescent protein expression in mouse ES cells, embryos, and adult animals. Genesis 40, 241–246 (2004). doi: 10.1002/gene.20095 [PubMed: 15593332]
55. Hughes ED et al. , Genetic variation in C57BL/6 ES cell lines and genetic instability in the Bruce4 C57BL/6 ES cell line. Mamm. Genome 18, 549–558 (2007). doi: 10.1007/s00335-007-9054-0 [PubMed: 17828574]
56. Townsend D, Witkop CJ Jr., J. Mattson, Tyrosinase subcellular distribution and kinetic parameters in wild type and C-locus mutant C57BL/6J mice. J. Exp. Zool 216, 113–119 (1981). doi: 10.1002/jez.1402160112 [PubMed: 6793688]
57. Riedl J et al. , Lifeact mice for studying F-actin dynamics. Nat. Methods 7, 168–169 (2010). doi: 10.1038/nmeth0310-168 [PubMed: 20195247]
58. Heit B, Kubes P, Measuring chemotaxis and chemokinesis: The under-agarose cell migration assay. Sci. STKE 2003, PL5 (2003).
59. Wang S, Dangerfield JP, Young RE, Nourshargh S, PECAM-1, alpha6 integrins and neutrophil elastase cooperate in mediating neutrophil transmigration. J. Cell Sci 118, 2067–2076 (2005). doi: 10.1242/jcs.02340 [PubMed: 15840647]
60. Dyer KD et al. , Functionally competent eosinophils differentiated ex vivo in high purity from normal mouse bone marrow. J. Immunol 181, 4004–4009 (2008). doi: 10.4049/jimmunol.181.6.4004 [PubMed: 18768855]
61. Davies DG et al. , The involvement of cell-to-cell signals in the development of a bacterial biofilm. Science 280, 295–298 (1998). doi: 10.1126/science.280.5361.295 [PubMed: 9535661]
62. Hoiseth SK, Stocker BA, Aromatic-dependent Salmonella typhimurium are non-virulent and effective as live vaccines. Nature 291, 238–239 (1981). doi: 10.1038/291238a0 [PubMed: 7015147]
63. Shakhar G et al. , Stable T cell-dendritic cell interactions precede the development of both tolerance and immunity in vivo. Nat. Immunol 6, 707–714 (2005). doi: 10.1038/ni1210 [PubMed: 15924144]

64. Evrard M et al. , Developmental Analysis of Bone Marrow Neutrophils Reveals Populations Specialized in Expansion, Trafficking, and Effector Functions. Immunity 48, 364–379. e8 (2018). doi: 10.1016/j.immuni.2018.02.002 [PubMed: 29466759]

65. Rada BK, Geiszt M, Káldi K, Timár C, Ligeti E, Dual role of phagocytic NADPH oxidase in bacterial killing. Blood 104, 2947–2953 (2004). doi: 10.1182/blood-2004-03-1005 [PubMed: 15251984]

66. Kienle K et al. , Data from “Neutrophils self-limit swarming to contain bacterial growth in vivo.” Zenodo (2021); DOI: 10.5281/zenodo.4709990.

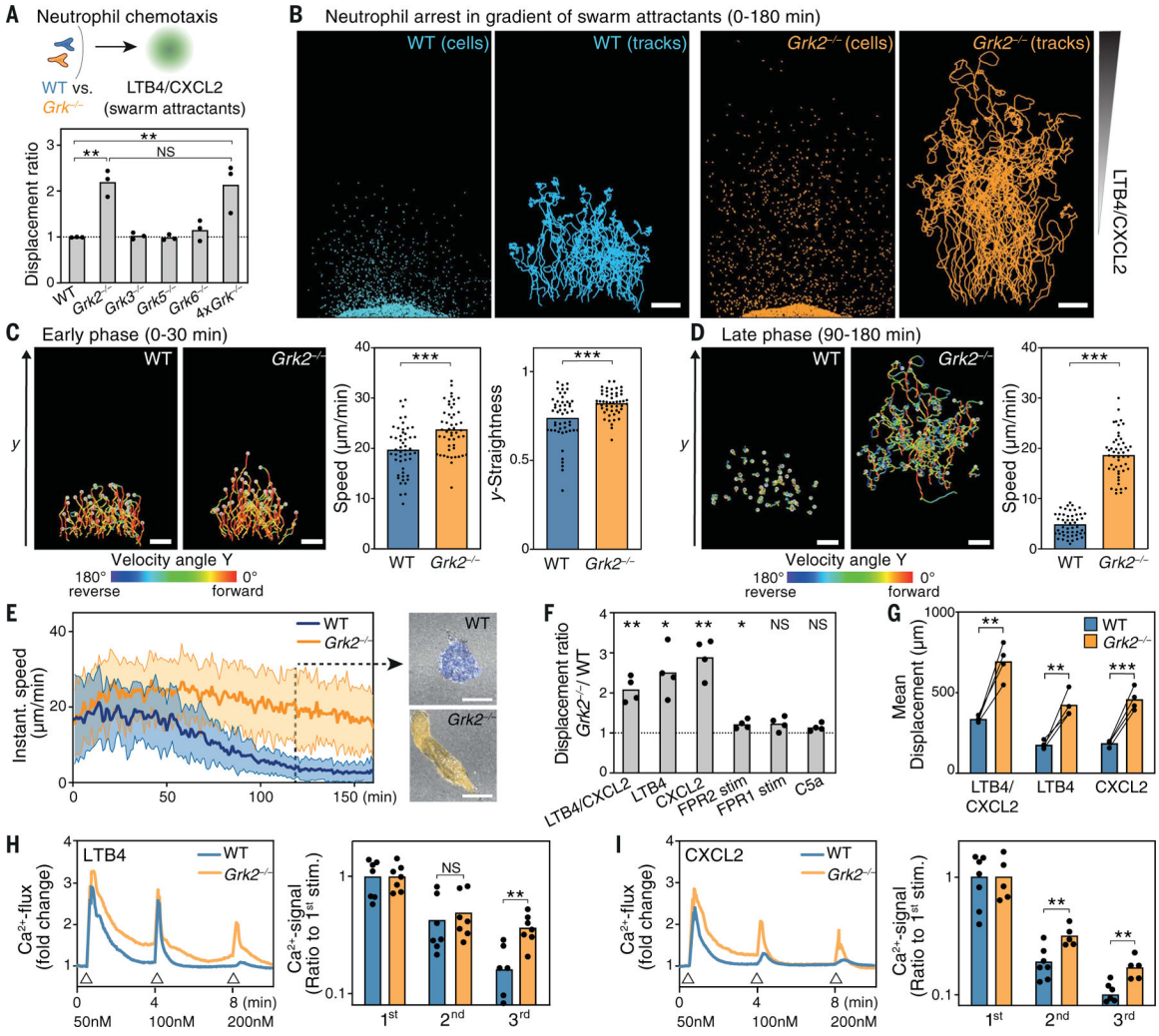


**Fig. 1. GRK2-dependent neutrophil arrest in fields of highly concentrated swarm attractants.**

(**A**) Comparative analysis of wild-type (WT) and *Grk*$^{-/-}$ neutrophils migrating side by side in an under-agarose assay setup along a combined gradient of the swarm attractants CXCL2/LTB4. *Grk*-deficient cells were lacking either an individual GRK or all four expressed GRKs (4×*Grk*$^{-/-}$). After 4 hours, migration endpoints were measured and are displayed as the ratio of *Grk*$^{-/-}$ to WT mean displacement. Bars display means of $n = 3$ biological replicates performed as independent experiments for each comparison. $^{**}P < 0.01$ (post hoc after ANOVA); NS, nonsignificant. (**B** to **E**) Migration of WT and *Grk2*$^{-/-}$ neutrophils toward CXCL2/LTB4 was recorded with live-cell microscopy to obtain cell tracks for 3 hours. From one representative experiment, 50 cells per genotype were tracked; cell displacement and full cell tracks after 3 hours are displayed in (B). The same cells were analyzed for migration and chemotaxis parameters during the early phase (0 to 30 min) (C) and the late phase (90 to 180 min) (D) of movement along the attractant gradient. The velocity angle $Y$ is the angle between the velocity vector and the $y$ axis (the axis of the attractant gradient); the $y$-straightness is the ratio of the displacement along the $y$ axis ($\Delta y$) to the total track length. In speed plot of (C), bars display means; $^{***}P < 0.001$ ($t$ test). In $y$-straightness plot of (C) and speed plot of (D), bars display median values; $^{***}P < 0.001$ ($U$ test). (E) Instantaneous

velocities with representative cell shapes at $t = 120$ min ($N = 50$ cells per genotype, means ± SD). (**F**) Comparative analysis of WT and *Grk2*$^{-/-}$ neutrophils migrating for 4 hours toward various attractive GPCR ligands, displayed as displacement ratio of *Grk2*$^{-/-}$ cells to WT cells. Bars display means of $n = 4$ biological replicates performed as independent experiments for each comparison. *$P < 0.05$, **$P < 0.01$ (one-sample $t$ test against 1). (**G**) Comparative analysis of WT and *Grk2*$^{-/-}$ neutrophil mean displacement in gradients of LTB4 and CXCL2, combined and separately. Bars display means of $n = 4$ biological replicates performed as independent experiments for each side-by-side comparison. **$P < 0.01$, ***$P < 0.001$ (ratio paired $t$ test). (**H** and **I**) Intracellular calcium flux analysis as a measure of GPCR desensitization. WT and *Grk2*$^{-/-}$ neutrophils were stimulated sequentially with increasing concentrations (as indicated) of either LTB4 (H) or CXCL2 (I) (triangles). Left panels: Real-time calcium flux of one experiment representative of $n = 5$ to 7 biological replicates for each genotype. Right panels: Quantification of the decrease in calcium signal after repeated attractant stimulation. Area under the curve (AUC) of the calcium signal was measured for individual stimulation peaks. Desensitization was measured as the ratio of the second and third stimulation values to the first stimulation in each independent experiment. The distribution of AUC values around the normalized average of the first stimulation is also displayed. Bars display means of $n = 5$ to 7 biological replicates for each genotype. **$P < 0.01$ ($t$ test). Scale bars, 500 μm [(B) to (D)], 10 μm (E).

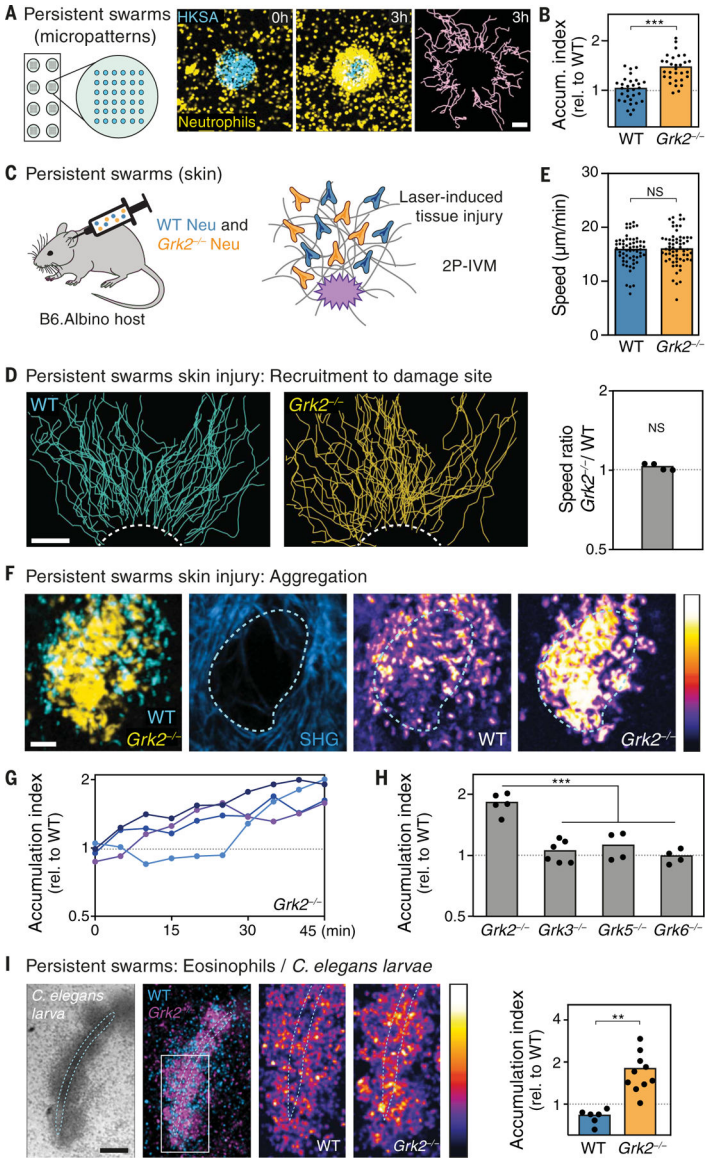


**Fig. 2. GRK2-dependent arrest in persistent swarms.**

**(A)** In vitro microscale array of patterned heat-killed *S. aureus* (HKSA) bioparticles (blue) to study persistent neutrophil swarms. Live microscopy of WT neutrophils (yellow) and cell tracking (pink) exemplifies swarming dynamics over 3 hours. (**B**) Analysis of neutrophil aggregation in clusters of two mixed populations, quantified as the WT/WT and $Grk2^{-/-}$/WT ratios of cells accumulating on HKSA spots (accumulation index) after 2 hours. Each dot represents one analyzed neutrophil cluster ($N = 30$) pooled from $n = 3$ biological replicates. Bars display means; $^{***}P < 0.001$ (*t* test). (C to G) 2P-IVM on ear dermis of anesthetized mice: Comparative analysis of persistent swarming after i.d. co-injection of WT and $Grk2^{-/-}$ neutrophils, which were differentially labeled with fluorescent dyes, into $Tyr^{c\text{-}2J/c\text{-}2J}$ (B6.Albino) mice. (C) Interstitial cell recruitment toward a laser-induced focal tissue injury. [(D) and (E)] For one representative experiment, the full cell tracks toward the damage site (dashed line) over the first 40 min after the initiation of the tissue damage

are displayed (D) and the cell speed analyzed [(E), top]. Each dot represents one tracked neutrophil ($N = 62$) from the side-by-side comparison of WT and *Grk2*$^{-/-}$ cells in one experiment. Bars display median values (*U* test). [(E), bottom] Comparative analysis of WT and *Grk2*$^{-/-}$ neutrophil speed during side-by-side chemotactic migration, displayed as the ratio of *Grk2*$^{-/-}$ to WT; $n = 4$ biological replicates (one-sample *t* test against 1). (F) Neutrophil aggregation was analyzed by 2P-IVM images at the endpoint of the clustering response when neutrophil recruitment ceases. In the representative example (see Movie 2, first part), neutrophil clustering is displayed 65 min after the initiation of tissue damage. (G) Aggregation in competitive clusters of *Grk2*$^{-/-}$ and WT cells was also quantified over time. Accumulation index was used as a quantitative parameter for neutrophil entry into the collagen-free wound center [cyan dashed line in (F)], displayed as the ratio of *Grk2*$^{-/-}$ to WT. Quantification began ($t = 0$) when small aggregates have already formed, which commonly occurs 5 to 20 min after the initial tissue injury depending on the individual experiment. Time courses of neutrophil clusters from $n = 4$ biological replicates (lines) are shown. (**H**) Quantification of endpoint neutrophil clustering after i.d. co-injection of WT cells and neutrophils lacking individual GRK family members into mice. The accumulation index (ratio of *Grk*$^{-/-}$ to WT) as a measure of aggregation was calculated when neutrophil recruitment had ceased and clusters stabilized. Each dot represents one analyzed neutrophil cluster ($N = 4$ to 6) pooled from $n = 2$ or 3 biological replicates. ***$P < 0.001$ (post hoc after ANOVA). (**I**) Comparative analysis of WT and *Grk2*$^{-/-}$ eosinophils forming persistent swarms around *C. elegans* dauer larvae (dotted line) in vitro. Confocal images illustrate endpoint eosinophil clusters after 2 hours. Each dot represents one analyzed eosinophil cluster ($N = 6$ to 10) pooled from $n = 3$ biological replicates. **$P < 0.01$ (*t* test). Scale bars, 100 μm [(A) and (I)], 50 μm (D), 30 μm (F). Bars with LUT color grading [(F) and (I)] display fluorescence signal intensities. SHG, second harmonic generation signal.

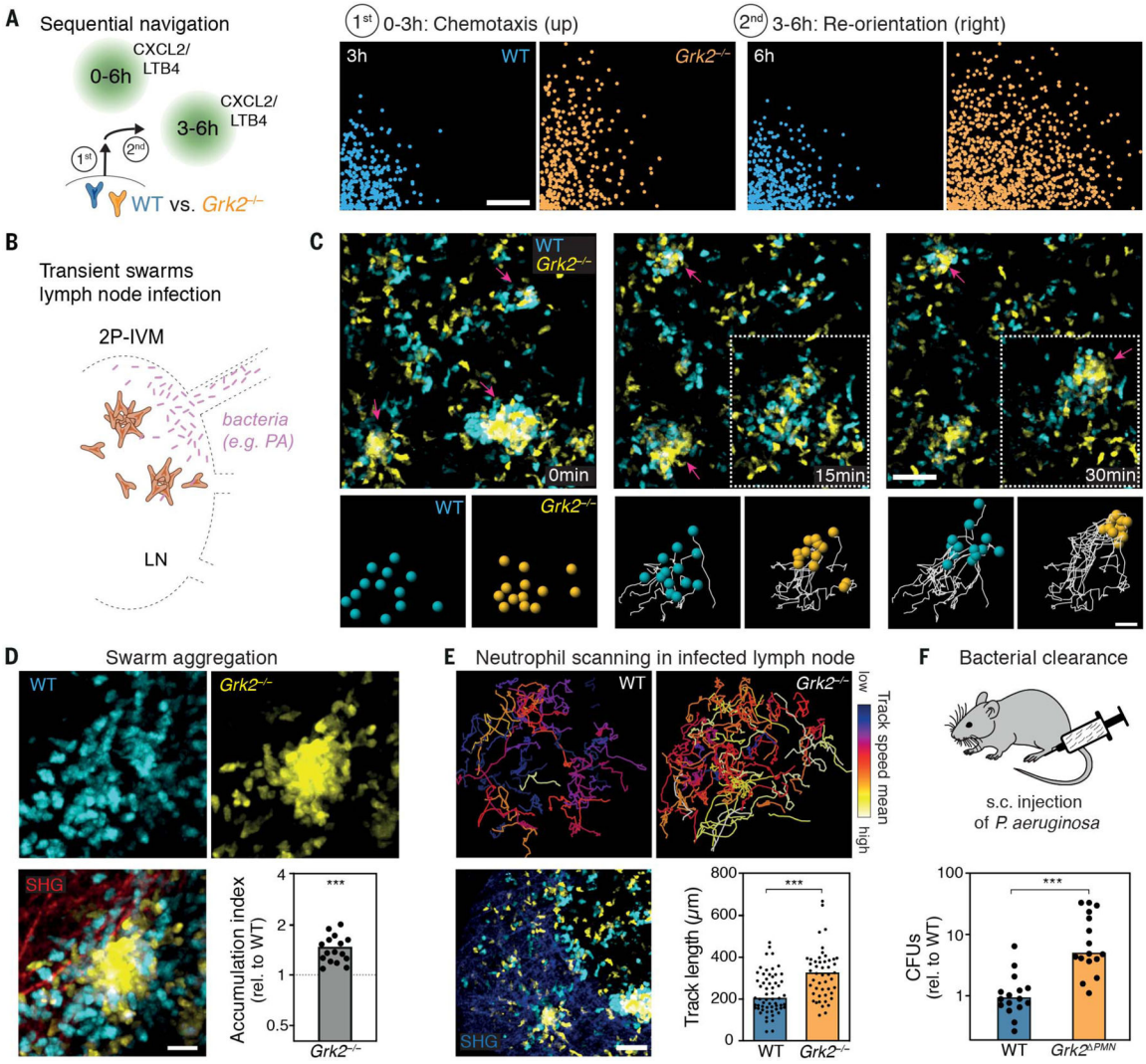


**Fig. 3. GRK2-controlled transient swarming restricts bacterial growth.**

(**A**) Left: Comparative analysis of sequential navigation behavior of WT and *Grk2*$^{-/-}$ neutrophils by exposing them to a first gradient of LTB4/CXCL2 and adding a second gradient of LTB4/CXCL2 at a 90° angle 3 hours later (right). Right: Cell positions after initial chemotaxis (3 hours) and reorientation (6 hours) were obtained by live-cell microscopy. (**B**) Mice were infected with bacteria in the footpad, and 2P-IVM of transient neutrophil swarms was then performed on draining popliteal lymph nodes. (**C** to **E**) Mice with mixed bone marrow [cyan, WT (*Ly6g*$^{Cre/+}$ *Rosa26*$^{LSL:Tom}$); yellow, *Grk2*$^{-/-}$ (*Mrp8-Cre Grk2*$^{fl/fl}$ *Lyz2*$^{Gfp/+}$)] were infected with *P. aeruginosa* (PA)–GFP before endogenous neutrophils were recorded 3 to 5 hours later. (C) Representative time-lapse sequence of neutrophil clusters (magenta arrows) in SCS. Bottom panels show migration tracks of neutrophils redirected to a second cluster (dotted box) with dragontails from $t = 0$ to 30 min. (D) 2P-IVM images show a representative neutrophil cluster of a transient swarm in the infected lymph node SCS. Quantification of neutrophil accumulation in transient clusters is displayed as the ratio of *Grk2*$^{-/-}$ to WT (see also materials and methods). Each dot represents one cluster ($N = 16$) pooled from $n = 4$ infected lymph nodes. ***$P < 0.001$

(one-sample *t* test against 1). (E) Trajectories of individual neutrophils are shown as tracks color-coded for mean track speed of cells (top), which navigate in the interstitial space of lymph nodes between neutrophil clusters (bottom). The color code ranges from 2 to 12 μm/min. Cell track lengths were quantified over 60 min; each dot represents one tracked neutrophil [$N = 59$ (WT), $N = 48$ ($Grk2^{-/-}$)] from one experiment. (**F**) Bacterial CFU counts of draining lymph nodes 8 hours after $Grk2^{\Delta PMN}$ and littermate control (WT) mice were infected with *P. aeruginosa*. Each dot represents one lymph node ($N = 16$) pooled from $n = 8$ mice for each genotype. In (E) and (F), bars display median values. ***$P < 0.001$ (*U* test). Scale bars, 1 mm (A), 50 μm [(C), top, and (E)], 20 μm [(C), bottom, and (D)]. SHG, second harmonic generation signal.

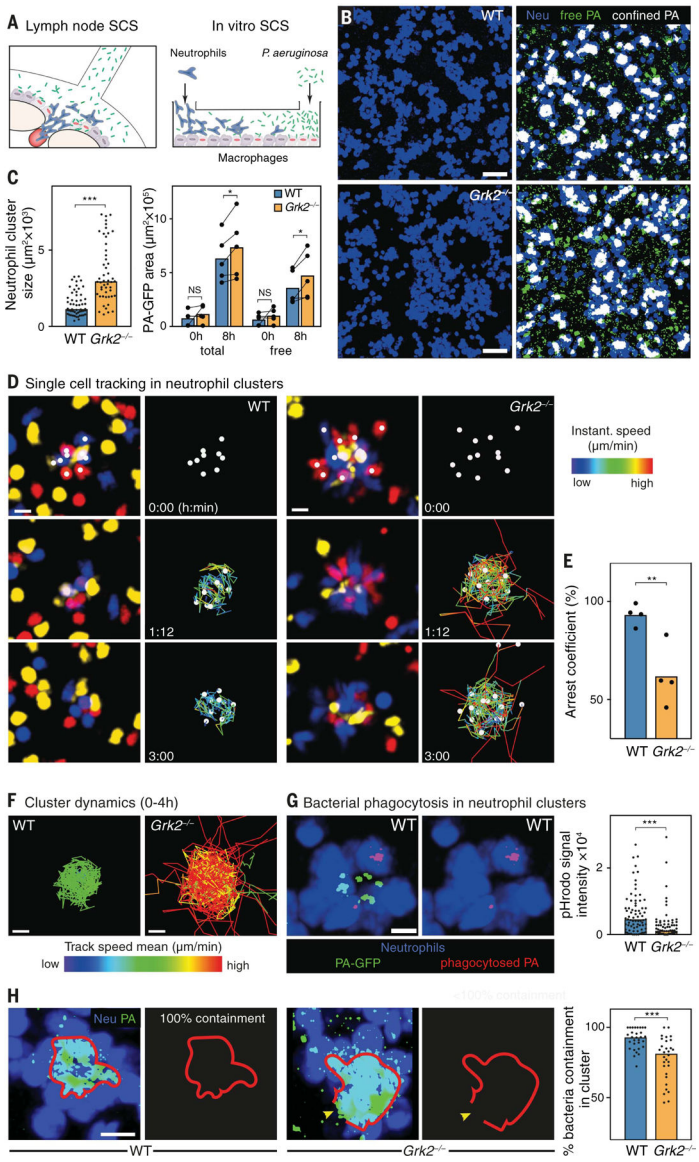


**Fig. 4. Neutrophil arrest is critical for containing bacteria in swarm clusters.**

(**A**) Coculture of neutrophils (blue), macrophages (gray), and *P. aeruginosa* PAO-1 expressing GFP (PA-GFP) (green) to mimic SCS lymph node infection in vitro. Red nuclei indicate dying macrophages. (**B**) WT or $Grk2^{-/-}$ neutrophils (Neu, blue) were separately cocultured with macrophages and PA-GFP (green). Fluorescent macrophages are not displayed. (**C**) After 8 hours of live-cell confocal microscopy, individual neutrophil cluster areas and PA-GFP signal areas were analyzed. For neutrophil cluster size (left), bars display median values; $N = 50$ to 55 clusters pooled from $n = 3$ biological replicates. $^{***}P < 0.001$ ($U$ test). For PA-GFP signal (right), total bacteria are the sum of neutrophil-contained bacteria (white) and bacteria outside of cell clusters (green, free). Bars display the mean; $n = 5$ biological replicates performed as independent experiments. $^{*}P < 0.05$ (ratio paired $t$ test). (**D**) Neutrophils of one genotype were triple dye–labeled to track neutrophils in cell clusters. Time sequences of representative WT (left) and $Grk2^{-/-}$ (right) neutrophil cluster dynamics

are shown. Trajectories of individual cells are shown as dragontails over 60 min and color-coded for instantaneous speed (ranging from 0 to 3.6 μm/min). (**E**) Arrest coefficient (percentage of instantaneous speed values less than 2 μm/min) was used as a quantitative parameter for neutrophil stopping at clusters. Bars display means; each dot represents one neutrophil cluster (with >7 cells tracked in each cluster) for each genotype from $n = 4$ biological replicates. $^{**}P < 0.01$ (*t* test). (**F**) Total 4-hour trajectories of individual cells are shown as tracks color-coded for mean track speed (ranging from 0 to 3.6 μm/min) in the neutrophil clusters of (D). (**G**) Left: Example of PA-GFP phagocytosis in WT neutrophil clusters. Right: PA-GFP was tagged with pHrodo dye to quantify the red signal of internalized bacteria in WT or *Grk2*$^{-/-}$ neutrophil clusters. Dots show analyzed neutrophil clusters ($N = 74$) pooled from $n = 3$ or 4 biological replicates. Bars display median values; $^{***}P < 0.001$ (*U* test). (**H**) Confocal images of representative WT and *Grk2*$^{-/-}$ clusters to quantify degrees of containment (red line; continuous = 100%) of PA-GFP (green) at 8 hours. Yellow arrowhead shows site of discontinuous containment. Dots show analyzed neutrophil clusters ($N = 30$) pooled from $n = 3$ biological replicates. Bars display median values; $^{***}P < 0.001$ (*U* test). Scale bars, 50 μm (B), 10 μm [(D), (F), (G), and (H)].

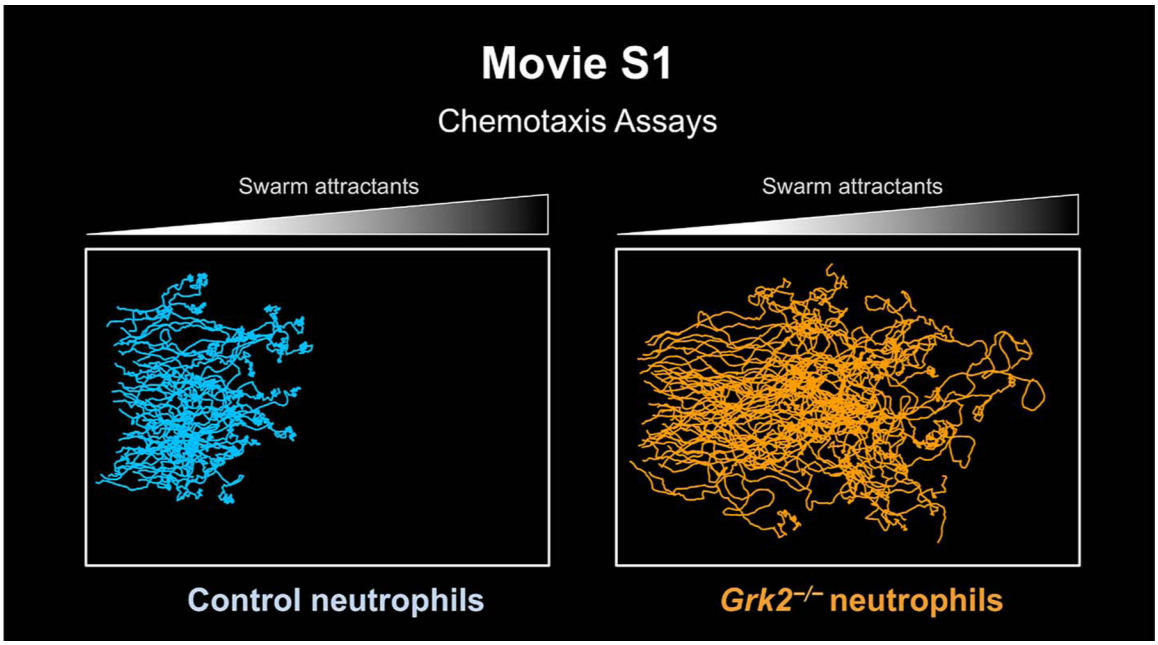


**Movie 1. Grk2$^{-/-}$ neutrophils continue to migrate in areas of highly concentrated swarm attractants.**

First part: Wild-type (WT) and *Grk2*$^{-/-}$ neutrophils were differentially dye-labeled and filled in a 1:1 ratio into one well (left) of an under-agarose chemotaxis assay setup. The swarm-mediating chemoattractants LTB4 (1 μM) and CXCL2 (1 μM) were filled into an opposite well to establish a gradient of increasing attractant concentrations (highest concentration at right). The representative video shows control (pseudo-colored in blue; upper panel) and *Grk2*$^{-/-}$ (pseudo-colored in orange; lower panel) neutrophils migrating toward the gradient (left to right). Graphic analysis of this experiment (Fig. 1, B to E, and fig. S1F) reveals that *Grk2*$^{-/-}$ neutrophils do not arrest, but continue to migrate at high concentrations of swarm attractants. Spinning-disk confocal microscopy ($x$, $y$ = 1070 μm, 870 μm; stitched from multi-tiled images), 10 frames/s. Time is displayed as hours:min. Second part: WT, *Grk2*$^{-/-}$, and 4×*Grk*$^{-/-}$ neutrophils were differentially dye-labeled and filled in a 1:1:1 ratio into one well (left) of an under-agarose chemotaxis assay setup with combined LTB4/CXCL2 gradient as in the experiment before. The representative video shows control (top), *Grk2*$^{-/-}$ (middle), and 4×*Grk*$^{-/-}$ (bottom) neutrophils migrating toward the gradient (left to right). Graphic analysis of this experiment (fig. S2F) reveals comparable migration of 4×*Grk*$^{-/-}$ and *Grk2*$^{-/-}$ neutrophils in swarm-attractant gradients. Spinning-disk confocal microscopy ($x$, $y$ = 1119 μm, 959 μm; stitched from multi-tiled images), 12 frames/s. Time is displayed as hours:min.

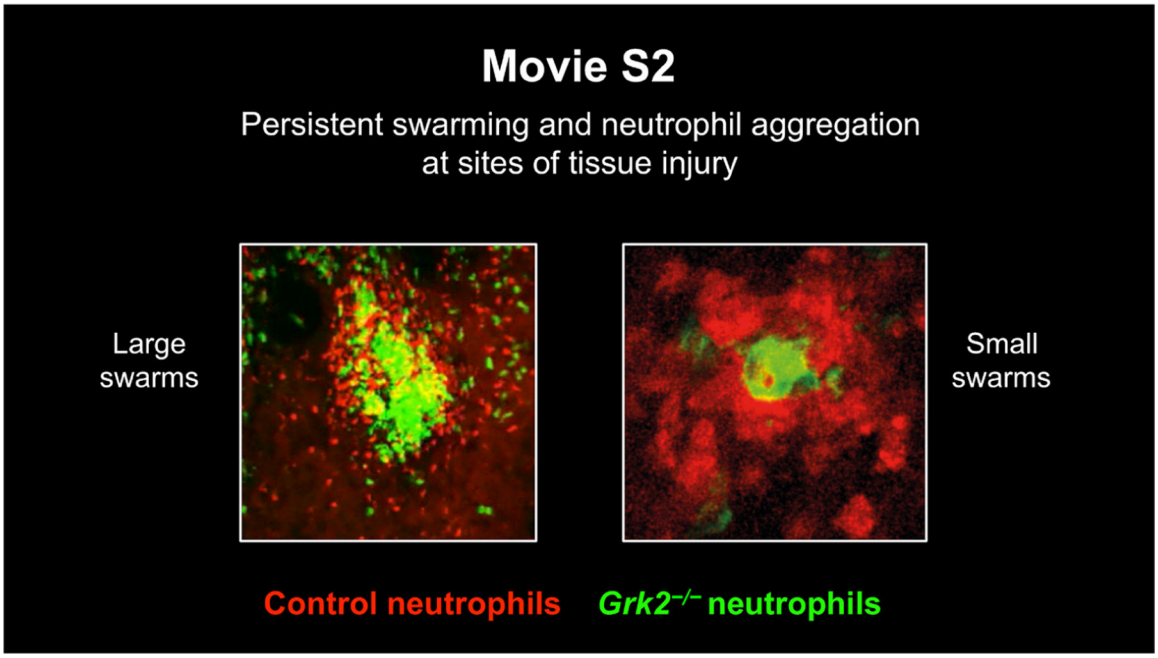


**Movie 2. GRK2-dependent neutrophil arrest in cell clusters of persistent swarms.**
First part (large neutrophil swarms): WT and *Grk2*$^{-/-}$ neutrophils were differentially dye-labeled and injected i.d. in a 1:1 ratio into the ventral ear skin of a *Tyr*$^{c\text{-}2J/c\text{-}2J}$ (B6.Albino) mouse 3 hours before laser-induced focal tissue damage (white circle at the start of the video). This representative video shows *Grk2*$^{-/-}$ (pseudo-colored in green) and control neutrophils (pseudo-colored in red) accumulating at the damage site in the skin dermis. Graphic analysis of the recruitment phase of several experiments (Fig. 2, D and E, and fig. S5, B and C) and analysis of the clustering response in this video (Fig. 2, F and G) reveal comparable recruitment of control and *Grk2*$^{-/-}$ neutrophils to the focal injury at early swarming phases. Over time, *Grk2*$^{-/-}$ neutrophils remain actively motile in growing clusters and dominate over control cells in the neutrophil cluster center. Two-photon intravital microscopy ($x$, $y$, $z$ = 512 μm, 512 μm, 12 μm; merge of $z$-stack), 18 frames/s. Time is displayed in minutes. Second part (small neutrophil swarms): Primary neutrophils were isolated from the bone marrow of *Grk2*$^{\Delta PMN}$ *Lifeact-GFP* mice and injected i.d. into the ventral ear skin of a *CAG-DsRed*$^{+/+}$ *Tyr*$^{c\text{-}2J/c\text{-}2J}$ mouse 3 hours before laser-induced focal tissue damage. This representative video shows the accumulation of *Grk2*$^{-/-}$ neutrophils (pseudo-colored in green) at a small cluster of endogenous WT neutrophils (pseudo-colored in red) that formed at the laser damage site. Analysis of the clustering response of several experiments, including comparison to control WT *Lifeact-GFP* neutrophil injection (fig. S5E) reveals that the continued motility of *Grk2*$^{-/-}$ neutrophils displaces control cells in the centers of small neutrophil clusters. Two-photon intravital microscopy ($x$, $y$, $z$ = 512 μm, 512 μm, 3 μm; merge of $z$-stack), 24 frames/s. Time is displayed in minutes. Third part (eosinophil swarms): GRK2 controls the accumulation of swarming eosinophils around worm larvae. WT and *Grk2*$^{-/-}$ eosinophils from IL-5 cultures of WT and *Vav-iCre Grk2*$^{fl/fl}$ mouse bone marrow, respectively, were differentially dye-labeled and placed in a 1:1 ratio with 4-day-old *C. elegans* dauer larvae in Matrigel. This representative video

shows the recording of bright-field (top left) and fluorescent microscopy (right) in which *Grk2*$^{-/-}$ (pseudo-colored in pink) and control (pseudo-colored in blue) eosinophils swarm and accumulate side by side around an individual larva. Analysis of eosinophil clustering of several experiments (Fig. 2I) reveals an increased clustering response of *Grk2*$^{-/-}$ eosinophils at the worm larva (dotted outline). Spinning-disk confocal microscopy ($x$, $y$ = 269 μm, 365 μm; stitched from multi-tiled images), 10 frames/s. Time is displayed as hours:min.

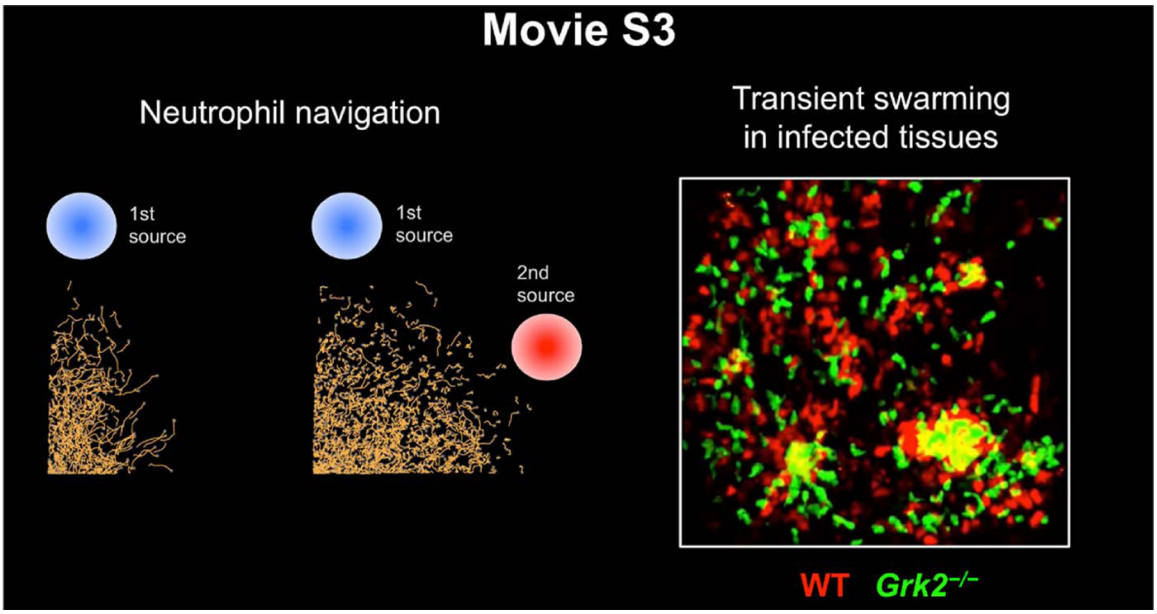


**Movie 3. GRK2 controls neutrophil arrest in transient swarm clusters and limits neutrophil space exploration in infected tissues.**

First part (in vitro): GRK2 limits neutrophil space exploration between competing gradients of swarm attractants. WT and *Grk2*$^{-/-}$ neutrophils were differentially dye-labeled and loaded in a 1:1 ratio into wells of a modified under-agarose assay setup that allows the analysis of neutrophil sequential navigation behavior in response to multiple attractant sources. Neutrophils were exposed to two spatiotemporally separated gradients of the swarm attractants LTB4 (1 μM) and CXCL2 (1 μM). First, *Grk2*$^{-/-}$ (pseudo-colored in orange) and WT neutrophils (pseudo-colored in blue) respond to a first gradient of LTB4/CXCL2 (gradient direction from top to bottom). The movie sequence shows side-by-side migration of tracked cells and starts 2 hours after the attractants were added. Second, WT and *Grk2*$^{-/-}$ neutrophils are redirected after 3 hours by an additional gradient of LTB4/CXCL2 at a 90° angle (gradient direction from right to left). This second movie starts immediately after attractants were added. Cell migration was tracked using Imaris spot function. Each circle indicates an individual neutrophil with motion paths as dragontails over the last 10 min (first movie) or 30 min (second movie) in the corresponding pseudo-color. Graphic analysis of this video (Fig. 3A and fig. S6, B and C) reveals that *Grk2*$^{-/-}$ neutrophils, in contrast to WT cells, were not desensitized by the first gradient and could be redirected by an additional gradient of the same attractants. Spinning-disk confocal microscopy ($x$, $y$ = 1682 μm, 1391 μm; stitched from multi-tiled images), 12 frames/s. Time is displayed as hours:min. Second part (*P. aeruginosa*–infected lymph node): GRK2 controls neutrophil arrest in transient swarm clusters in vivo. Mice with mixed bone marrow [*Ly6g*$^{Cre/+}$ *Rosa26*$^{LSL:Tom}$ (WT) pseudo-colored in red; *Mrp8-Cre Grk2*$^{fl/fl}$ *Lyz2*$^{Gfp/+}$ (*Grk2*$^{-/-}$) pseudo-colored in green] were injected with *P. aeruginosa* (PA)–GFP (fluorescence not visible here) into the footpad before endogenous neutrophils were recorded 3 to 4 hours later. Two-photon intravital microscopy of transient neutrophil swarms was performed on the SCS of draining popliteal lymph nodes. This representative video shows *Grk2*$^{-/-}$ (pseudo-colored in green) and control neutrophils (pseudo-colored in red) side by side during the formation and

disappearance of transient neutrophil swarm clusters. Arrows indicate neutrophil clusters; the pink arrow highlights neutrophil migration out of one cluster to a newly developing cluster. Static images of this video are presented in Fig. 3C. Graphic analysis of several experiments (Fig. 3D) reveals that *Grk2*$^{-/-}$ neutrophils dominate over control cells in the central regions of newly forming clusters. Moreover, *Grk2*$^{-/-}$ neutrophils also migrate rapidly out of clusters again and become redirected to the centers of newly developing clusters. Two-photon intravital microscopy (*x*, *y*, *z* = 504 μm, 404 μm, 14 μm; merge of *z*-stack), 12 frames/s. Time is displayed in minutes. Third part (*S. typhimurium*–infected lymph node): Mice with mixed bone marrow [*Ly6g*$^{Cre/+}$ *Rosa26*$^{LSL:Tom}$ (WT) pseudo-colored in red; *Mrp8-Cre Grk2*$^{fl/fl}$ *Lyz2*$^{Gfp/+}$(*Grk2*$^{-/-}$) pseudo-colored in green] were injected with *S. typhimurium* into the footpad; endogenous neutrophils were recorded 3 to 4 hours later. Two-photon intravital microscopy of transient neutrophil swarms was performed on the SCS of draining popliteal lymph nodes. This representative video shows *Grk2*$^{-/-}$ (in green) and control neutrophils (in red) side by side during the formation and disappearance of transient neutrophil swarm clusters (arrows). Static images of this video and graphic analysis of several experiments (fig. S6, E and F) reveal that *Grk2*$^{-/-}$ neutrophils dominate over control cells in the central regions of newly forming clusters during *S. typhimurium* infection. Moreover, *Grk2*$^{-/-}$ neutrophils migrate rapidly out of clusters again, have increased interstitial speed, and become redirected to the centers of newly developing clusters. Two-photon intravital microscopy (*x*, *y*, *z* = 512 μm, 512 μm, 10 μm; merge of *z*-stack), 12 frames/s. Time is displayed in minutes. Fourth part (*P. aeruginosa*–infected lymph node): GRK2 limits neutrophil space exploration in infected lymph node tissue. Cell tracking of endogenous WT and *Grk2*$^{-/-}$ neutrophils that migrate side by side in the interstitial areas of a *P. aeruginosa*–infected lymph node (image insert, tissue region as in second part of this video). This representative video shows the interstitial scanning behavior of *Grk2*$^{-/-}$ (pseudo-colored in green) and control neutrophils (pseudo-colored in red) with motion paths over the last 15 min as dragontails in the corresponding pseudo-color. At the end, the total trajectories of individual neutrophils after 60 min are shown as tracks color-coded for average speed. Graphic analysis (Fig. 3E) reveals that neutrophils lacking GRK2 show increased tissue scanning but impaired migration arrest during interstitial movement in infected lymph nodes. Cell tracking based on two-photon intravital microscopy, 10 frames/s. Time is displayed in minutes.

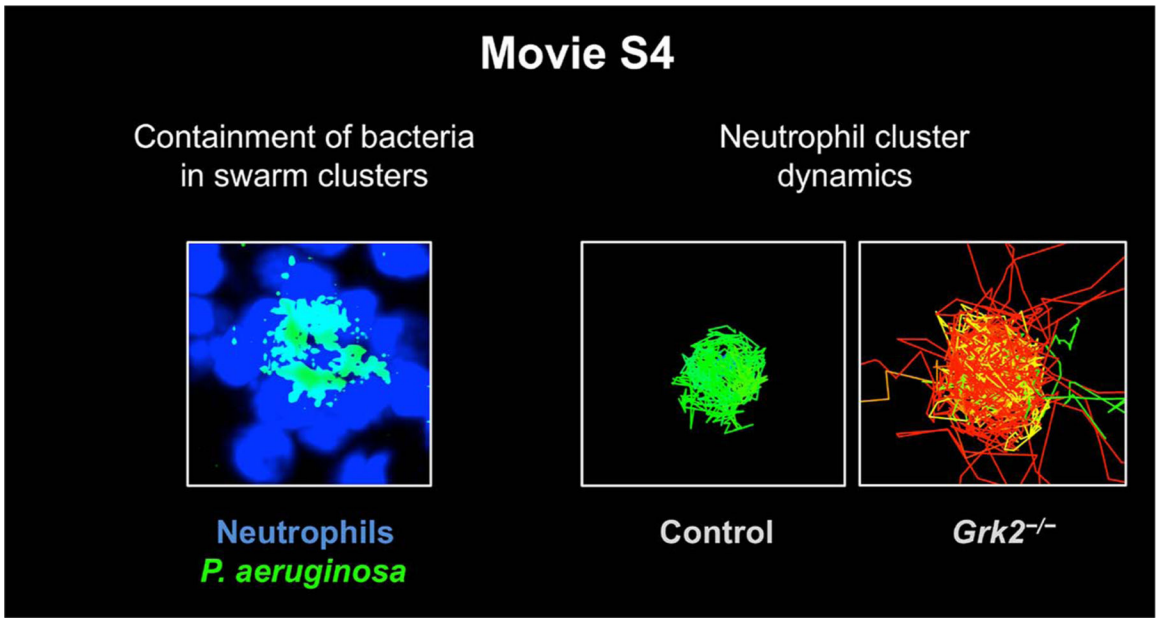


**Movie 4. GRK2 controls arrest to form stable neutrophil clusters in order to contain bacterial growth.**

First part: Swarm-like dynamics of *P. aeruginosa* precede macrophage death in vitro. Bone marrow–derived macrophages were fluorescently labeled with CellTracker Blue and co-incubated with *P. aeruginosa* PAO-1 expressing GFP (PA-GFP). This representative video shows macrophages (pseudo-colored in violet) and PA-GFP (pseudo-colored in green) in the presence of propidium iodide as marker for dying cells (pseudo-colored in red), and reveals pack-swarming bacteria that precede macrophage cell death at local sites. Right panels show zoom-in on dying macrophage clusters. Static images of this video and the quantification of macrophage survival of several experiments are shown in fig. S7, B and C. Laser-scanning fluorescence confocal microscopy (*x*, *y*, *z* = 1024 μm, 1024 μm, 4 μm; merge of *z*-stack), 12 frames/s. Time is displayed in minutes. Second part: *Grk2*$^{-/-}$ neutrophils form larger clusters but show impaired control of bacterial growth. To mimic a bacterial infection of the lymph node SCS in vitro, we co-incubated bone marrow–derived macrophages with PA-GFP in the presence of either *Grk2*$^{-/-}$ or WT neutrophils. This video shows representative experiments in which the swarming dynamics of WT and *Grk2*$^{-/-}$ neutrophils (pseudo-colored in blue) and bacteria (pseudo-colored in green) are shown together at left, and bacteria fluorescence signal alone at right. Macrophages were present but are not displayed here. Graphic analysis of several experiments (Fig. 4, B and C) reveals increased growth of bacteria in experiments with *Grk2*$^{-/-}$ neutrophils in comparison to control cells, in particular in the extracellular space between neutrophil clusters.Laser-scanning fluorescence confocal microscopy (*x*, *y*, *z* = 513 μm, 513 μm, 4 μm; merge of *z*-stack), 20 frames/s. Time is displayed as hours:min. Third part: GRK2 controls neutrophil arrest to form stable swarm clusters. Bone marrow–derived macrophages were co-incubated with PA-GFP in the presence of either *Grk2*$^{-/-}$ or WT neutrophils. Neutrophils of one genotype were split into three fractions and differentially labeled with three dyes (CellTracker Blue, 5-TAMRA, CellTracker Far Red) before they were pooled and added to the coculture. Triple-color labeling allowed

the identification and single-cell tracking of neutrophils in dense cell clusters. This video shows representative neutrophil dynamics in one *Grk2*$^{-/-}$ or WT clusters (left), together with single-cell motion tracks over the last 45 min as red dragontails and tracked cells as white circles (right). Graphic analysis of several experiments (Fig. 4, D to F, and fig. S7F) reveals that *Grk2*$^{-/-}$ neutrophils lack arrest phases at clusters and move rapidly out of them again, resulting in unstable neutrophil aggregates. Laser scanning confocal microscopy (*x*, *y*, *z* = 89 μm, 78 μm, 6 μm; merge of *z*-stack), 15 frames/s. Time is displayed as hours:min.